AN ABSTRACT OF THE THESIS OF

Paul Edward Keary for the degree of Master of Science in Mechanical Engineering presented on April 26, 1984

Title: A Comparison of Experimental Mode I Analysis Methods for the Interlaminar Fracture Toughness Characterization of Graphite/Epoxy Composite Materials

Abstract approved: Redacted for Privacy
Tim C. Kennedy

Three approaches for evaluating mode I interlaminar strain energy release rates in graphite/epoxy composites were compared using experimental data from double cantilever beam specimens. Expressions for evaluating strain energy release rates were arrived at based on assumptions regarding specimen geometry and material behavior. The calculations included the direct method of the J integral approach, a compliance calibrated approach and an analytical equation derived from small deflection, linear beam bending theory. The J integral approach accounts for both linear and nonlinear material response, whereas the compliance calibrated and linear beam bending methods assume linear material behavior.

Experimental observations of several material systems indicated a nonlinear elastic material response. Interlaminar strain energy release rates were found to be overestimated by methods assuming linear material behavior. Permanent deflection was seen to accumulate in the arms of

the double cantilever beam specimen as the crack surface area increased. This component of deflection must be accounted for in all forms of analysis when using double cantilever beam specimens.

A COMPARISON OF EXPERIMENTAL MODE I ANALYSIS METHODS FOR THE INTERLAMINAR FRACTURE TOUGHNESS CHARACTERIZATION OF GRAPHITE/EPOXY COMPOSITE MATERIALS

by

PAUL EDWARD KEARY

A THESIS

submitted to

Oregon State University

in partial fulfillment of
the requirements for the
degree of

Master of Science

Completed April 26, 1984

Commencement June 1984

APPROVED:

Redacted for Privacy

Professor of Mechanical Engineering in charge of major

Redacted for Privacy

Head of Department of Mechanical Engineering

Redacted for Privacy

Dean of Graduate School

Date thesis is presented April 26, 1984

Typed by Penny Williams for Paul Edward Keary

Acknowledgements

This thesis is dedicated to my mother and father for their love and encouragement throughout the years. I would also like to thank the Boeing Commercial Airplane Company for their support of the work from which this thesis evolved. Finally, I would like to thank Dr. Tim Kennedy, Dr. Mysore Narasimhan, Dr. Jim Wilson, and my colleagues Larry Ilcewicz, Casey Shaar, and Jess Trostle for their insight and help in making this program a success.

Table of Contents

List of Figures

A COMPARISON OF EXPERIMENTAL MODE I ANALYSIS METHODS FOR THE INTERLAMINAR FRACTURE TOUGHNESS CHARACTERIZATION OF GRAPHITE/EPOXY COMPOSITE MATERIALS

Introduction

During recent years the increased use of newer lightweight materials has brought about a considerable amount of work among scientists and engineers dealing with characterizing these materials in terms of their strength properties. The complexity of some of these newer materials, such as polymers and composites, presents a variety of challenging problems to research scientists. Questions as to why materials fail when subjected to relatively low stresses have brought about many theories dealing with material behavior on both the macroscopic and microscopic scales.

During the past 30 years the study of fracture mechanics has continually evolved to include many types of engineering materials. The original concepts of fracture mechanics were based on materials that fail in a brittle isotropic manner. This is often referred to as Linear Elastic Fracture Mechanics (LEFM). However, with the evolution of the aircraft and space industries, the need for newer, lightweight, fuel efficient structures has brought about materials that do not always follow LEFM concepts. Materials such as polymers and composites often possess nonlinear or elastic-plastic material behavior. The need to understand failure mechanisms of these types of materials has resulted in a refining of fracture analysis methods.

Initial attempts to extend fracture mechanics concepts began with plasticity corrections to LEFM methods. These methods have been

somewhat successful in dealing with materials exhibiting small-scale crack tip plasticity. However, for large scale crack tip placticity these corrections have been proven to be insufficient[28].

Other attempts at developing elastic-plastic models have consisted of Crack Opening Displacement (COD) methods and Equivalent Energy (EE) concepts. These methods however, are somewhat lacking of a rational physical and analytical basis and, therefore, application of these methods have always been suspect.

The most recent attempt to extend fracture mechanics concepts has been the J-integral approach. The development of the J-integral has allowed research scientists to examine failure mechanisms of materials which exhibit highly plastic crack tip behavior. It possesses both a rational analytical and physical basis equally as powerful as LEFM concepts. In fact, the J-integral method is often viewed as a direct extension of the methods of LEFM into the elastic-plastic and fully plastic regimes.

Objectives

One of the primary goals of this research has been to develop a consistent, reliable and accurate method of obtaining fracture toughness data of graphite/epoxy composite materials. The J-integral approach along with methods using LEFM concepts have been examined. Experimental results of over 90 composite specimens tested under Mode I conditions are presented.

It is first necessary to develop an understanding of the physical and mechanical properties of graphite epoxy composite materials. This is presented in the following section.

A review of the literature will be given to cover fundamental concepts of fracture mechanics. First, the development and use of LEFM and elastic-plastic fracture mechanics concepts is presented. Second, the experimental methods used to measure fracture toughness in conventional materials (e.g. metals) is explained. These methods along with those utilizing a double cantilever beam (DCB) specimen as applied to measuring interlaminar fracture toughness in composite materials is examined. Third, the review of literature will cover the importance of recognizing material behavior and its effects on obtaining qualitative measures of critical energy release rates.

The next sections will cover the analytical and experimental methods which were used to determine critical energy release rates for the composite materials examined in this study. Three separate analytical expressions for evaluating critical energy release rates utilizing a double cantilever beam specimen are presented. Assumptions made in deriving each expression will be examined in this section.

Finally, results of mode I interlaminar fracture toughness tests

of the composite DCB specimens examined in this study are included. A discussion of analysis methods which assume linear elastic, nonlinear elastic or elastic-plastic material behavior as pertaining to composite materials is presented. Conclusions regarding which analysis method best characterize critical energy release rates in composites are based on experimental observations of material behavior.

Structural Aspects of Graphite/Epoxy Composite Materials

With the development of composite materials as secondary and, in some instances, primary load carrying structural components many questions pertaining to the mechanical and physical nature of composites have emerged. Because of the complex physical makeup of composite materials, structural analysis methods have proved to by very difficult to understand. As a result, many engineers have reverted to the idea of treating composites as homogeneous isotropic materials with the mechanical properties dependent on the composite layup. This often results in designs which do not utilize the maximum structural performance of these materials. Hopefully, in the near future, with the use of advanced theories which characterize composites on both a macroscopic and microscopic scale, the maximum structure performance of these materials will be attainable. When the full advantages of composite materials are utilized, both the aircraft and spacecraft industry will design structures in a manner much different from the present.

Composite materials may be classified as three types. First there are particulate composites which consist of one or more materials suspended in a matrix of another material. Concrete may be thought of as a particulate composite. Second, there are laminated composites consisting of layers of various materials that are bonded together, such as plywood, for example. Finally, there are fibrous composites which are composed of continuous fibers that are bonded together in a resin matrix.

Composite materials are often composed of a combination of two or three of the above types. For example, a laminated fiber reinforced

composite consists of plies of continuous fibers bonded together in a matrix and layered to form a structural material. One ply by itself is often referred to as a lamina whereas a number of plies bonded together are referred to as a laminate.

The fibers which are used in laminated fiber reinforced composites consists of many different types. Fiberglass, kevlar, and graphite are but a few. There are also a number of different types of resins which may be used to form the matrix. Resins are normally very brittle in nature, although depending on the service requirements, somewhat ductile resins are sometimes used. The choice of the specific types of fiber and resin usually depends upon cost, weight, and required structural integrity.

There are many advantages to using laminated fiber reinforced composites as structural components. The main advantage is the high stiffness-to-weight ratios that fiber reinforced composites have to offer. On an equal weight basis fiber reinforced composites have been known to be as much as five times as strong as steel[41]. They also have superior corrosion resistance along with the ability to dissipate static electrical charge which makes them especially marketable for harsh environmental conditions. Another advantage is the ability for the designer to orient the material according to the stresses in a structural member. The structural properties of continuous carbon fibers are parallel to the longitudinal axis of the fibers. This structural tailoring permits greater design efficiency as compared to conventional designs with basically isotropic metals or plastics.

On the other hand, despite its many advantages, fiber reinforced composites have a number of disadvantages. The primary disadvantage is

the fact the strength properties transverse to the longitudinal direction are poor. This often results in delaminations and interlaminar failure. Current cost of high-strength carbon fibers is high, ranging from $20 to $30 per pound, although this is expected to decrease in the near future. Another disadvantage is the anisotropic properties of fiber reinforced composites. The testing and analysis methods for such materials are very difficult to perform.

The physical makeup of laminated fiber reinforced composites consists of a number of plies or laminas layed to form what is called a laminate. An example of a typical layup is shown in Figure 1. Since the fibers are the primary load carrying component, the laminates are usually constructed with varying fiber orientations to account for various loading conditions. The main purpose of the matrix is to hold the fibers in place and to transfer stresses among the fibers. The lay-up selection is designed to tailor the directional dependence of strength and stiffness of a material to match the loading environment of a particular structural element. This enables the engineer to design a part to match the service loads it will be subjected to. Shearing and out of plane normal stresses often arise from the tendency of each layer to deform independently of its neighboring layers. These stresses must be considered in the overall design of the part to avoid delaminations and cracking along the ply interfaces. Therefore, the stacking sequence plays a primary role in the effectiveness of the overall strength of the structural element.

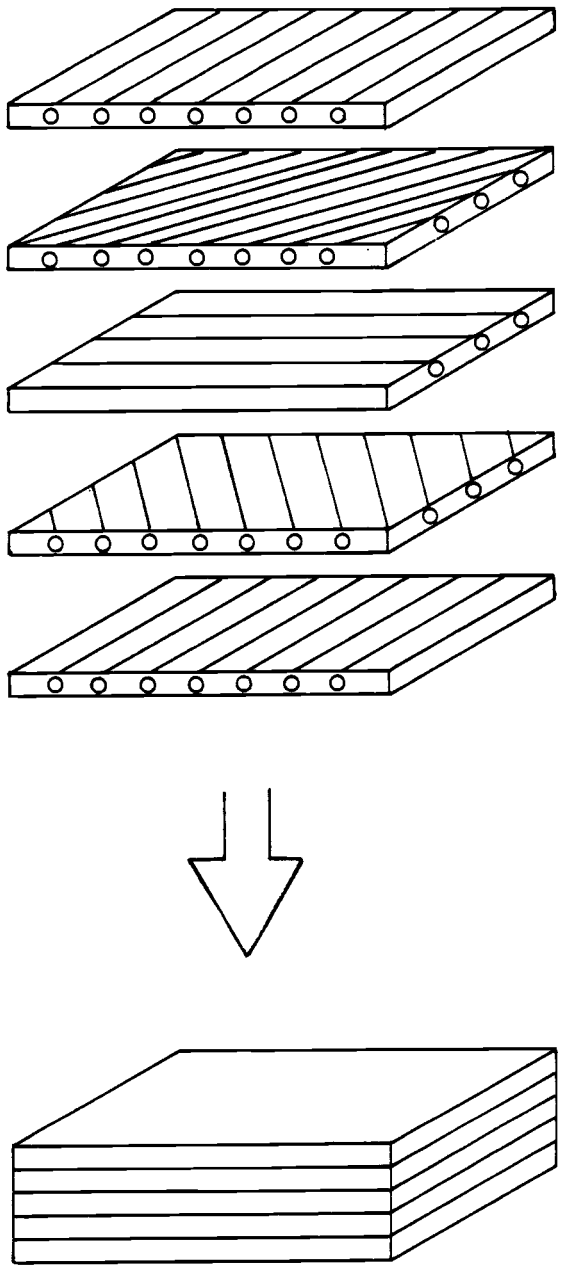

Figure 1. Schematic drawings showing the individual laminas and a laminate.

Review of Literature

The Griffith Approach to Brittle Fracture

Approximately 60 years ago A.A. Griffith developed a theory dealing with the fracture of cracks embedded in brittle solids[12]. His approach for the formulation of a brittle fracture criteria was through the use of the "theorem of minimum energy." Simply stated, this theorem represents the condition that the potential energy in a system is a minimum if the stressed elastic body is in a state of equilibrium. For completely brittle elastic solids (neglecting plastic flow at the crack tip) potential energy may be regarded as surface energy. Griffith believed that the equilibrium condition was reached when fracture of a solid, under a given stage of loading, had occurred. In order for fracture to occur under the action of external loads in an elastic condition the strain energy, W, supplied to the system must reach a point where it is equal to the increase in surface energy, U, due to the formation of the new cracked surface. Hence, assuming elastic behavior, the total decrease in potential energy due to the formation of a crack is equal to the increase in strain energy, W, minus the increase in surface energy, U. Griffith stated that the potential energy, U, of the surface of the crack, per unit thickness was

$$U = 4aT \qquad (1)$$

where T is the surface tension of the material and 4a is the crack length (2a) x 2 surface areas.

To determine the strain energy, W, Griffith used C.E. Inglis'[16] stress analysis approach for stresses in an infinitely large plate containing an elliptical crack as shown in Figure 2.

The increase in strain energy, W, due to the presence of a crack was determined to be

$$W = \frac{(3 - p)\ \pi\ a^2\ \sigma^2}{8\mu} \qquad (2)$$

per unit thickness of material where 2a is the crack length, σ is the applied stress, μ is the shear modulus and p is a function of Poissons' ratio, ν , which takes on a different form depending on whether the condition is either plane stress or plane strain.

The condition at which crack extension will occur is

$$\frac{\partial}{\partial a}(W - U) = 0 \qquad (3)$$

Griffith then performed the operation and obtained plane stress and plane strain expressions for the critical breaking stress, σ. These were later found to be in error due to a slight mismatch of the solution for stresses in Inglis' equation and the boundary conditions. In 1924 Griffith[13] corrected the stress criteria and obtained

$$\sigma = \sqrt{\frac{2ET}{\pi a(1 - \nu^2)}} \qquad \text{for plane strain} \qquad (4a)$$

$$\sigma = \sqrt{\frac{2ET}{\pi a}} \qquad \text{for plane stress} \qquad (4b)$$

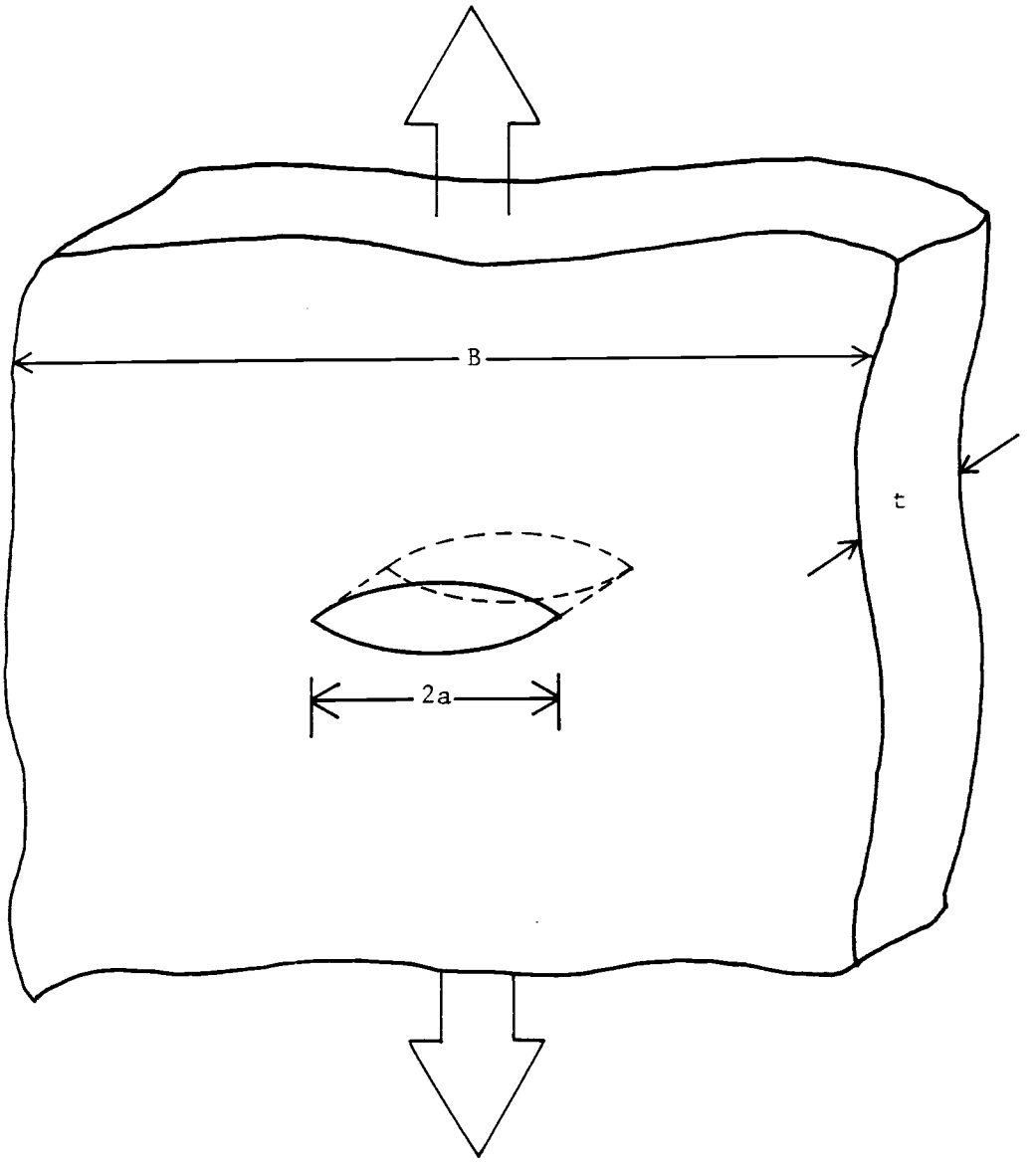

Figure 2. Through the thickness crack in a large plate.

where E is Young's modulus.

Because of this correction the strain energy term $\frac{\partial W}{\partial a}$, becomes

$$\frac{\partial W}{\partial a} = \frac{2 \pi \sigma^2 a}{E} \qquad (5)$$

per unit plate thickness. Usually, $\frac{\partial W}{\partial a}$ is replaced by G to obtain

$$G = \frac{\partial W}{\partial a} = \frac{\pi \sigma^2 a}{E} \qquad (6)$$

where G is referred to as the crack driving force or elastic energy release rate per crack tip. The second term in Equation 3, $\frac{\partial U}{\partial a}$, is often referred to as the crack resistance force, R. This is the energy consumed in crack propagation. For very brittle materials, such as glass, this consists of surface energy only. However, for ductile materials such as metals, the plastic deformation occurring at the crack tip will add to the surface energy term making it larger. As a result, the original Griffith criteria presented here, is only valid if the material retains a brittle elastic nature. Consequently, this also implies that the crack tip radius is assumed to be very sharp.

Griffith went on to experimentally verify the accuracy of the stress criteria equations. As a material to use, he selected glass because it was known to be a brittle isotropic material whose surface tension at ordinary temperatures could be estimated. Direct determinations of the surface tension, however, were found to be impractical and ultimately an indirect approach was decided on. This was performed by experimentally determining the surface tension for glass at a number of high temperatures. By extrapolation, values at

ordinary temperatures were determined.

Griffith then conducted experiments using thin round tubes and spherical bulbs which were deliberately cracked, annealed, and then fractured by internal pressure. The specimens were annealed to eliminate any residual stresses associated with the cracking process.

The results from Griffith's experiments were found to be in favorable agreement with his theoretical predicted results. He concluded that the theorem of minimum potential energy could be extended to be capable of predicting the breaking loads of elastic solids, provided the increase of surface energy which occurs during formation of cracks is taken into account[12]. Thus, Griffith's work has become the basis for research in the field of brittle fracture.

Modifications of the Griffith Approach

As previously mentioned, an important assumption made in developing the Griffith fracture criteria is that it is only valid for materials that exhibit elastic behavior at the crack tip. Most materials contain differences in behavior not initially accounted for in the formulation of the Griffith problem. Plastic flow in the vicinity of the crack tip is one example. Orowan[27] recognized this fact and made modifications to Griffith's work for application to low carbon steels that show plastic deformation in a small region near the crack tip. Orowan replaced the surface energy term found in Griffith's equation by a plastic work that corresponds to behavior at the crack tip. He showed that the energy concept used by Griffith is only valid if plastic deformation is either absent or confined to a thin layer of material at the fracture surface so that the bulk of the specimen

remained elastic. For materials that exhibit ductile fracture, Orowan showed Griffith's theory to be invalid.

Irwin[17] also considered modification of Griffith's theory of materials capable of plastic deformation at the crack tip. He was responsible for the introduction of the strain energy release rate (G) and the stress intensity factor (K). These were shown to be functions of test configuration, load, crack length, and material constants. Both the strain energy release rate and the stress intensity factor are useful in providing measures of brittle fracture resistance in the presence of localized plastic effects because they are easily obtained by experiment.

Irwin's approach to a failure criterion examined the stress field in the immediate vicinity of a crack tip as opposed to considering the energy of the entire system. He considered the crack tip region of a "somewhat brittle" crack to be a region where large plastic deformations may exist close to the crack tip but not extending away from the crack by more than a small fraction of the total crack length[17]. Irwin observed that there exists three independent kinematic movements of the upper and lower crack surfaces as shown in Figure 3. These three basic types of deformations are the necessary and sufficient conditions which describe all the possible modes of failure for the most general state of elastic stress[34]. In reality, in-service failures normally occur due to a combination of two or all three of these modes. Independently these failure modes may be described as follows:

Mode I: Opening Mode (Figure 3A). The displacements of the crack surfaces are perpendicular to the plane of the crack. The motions

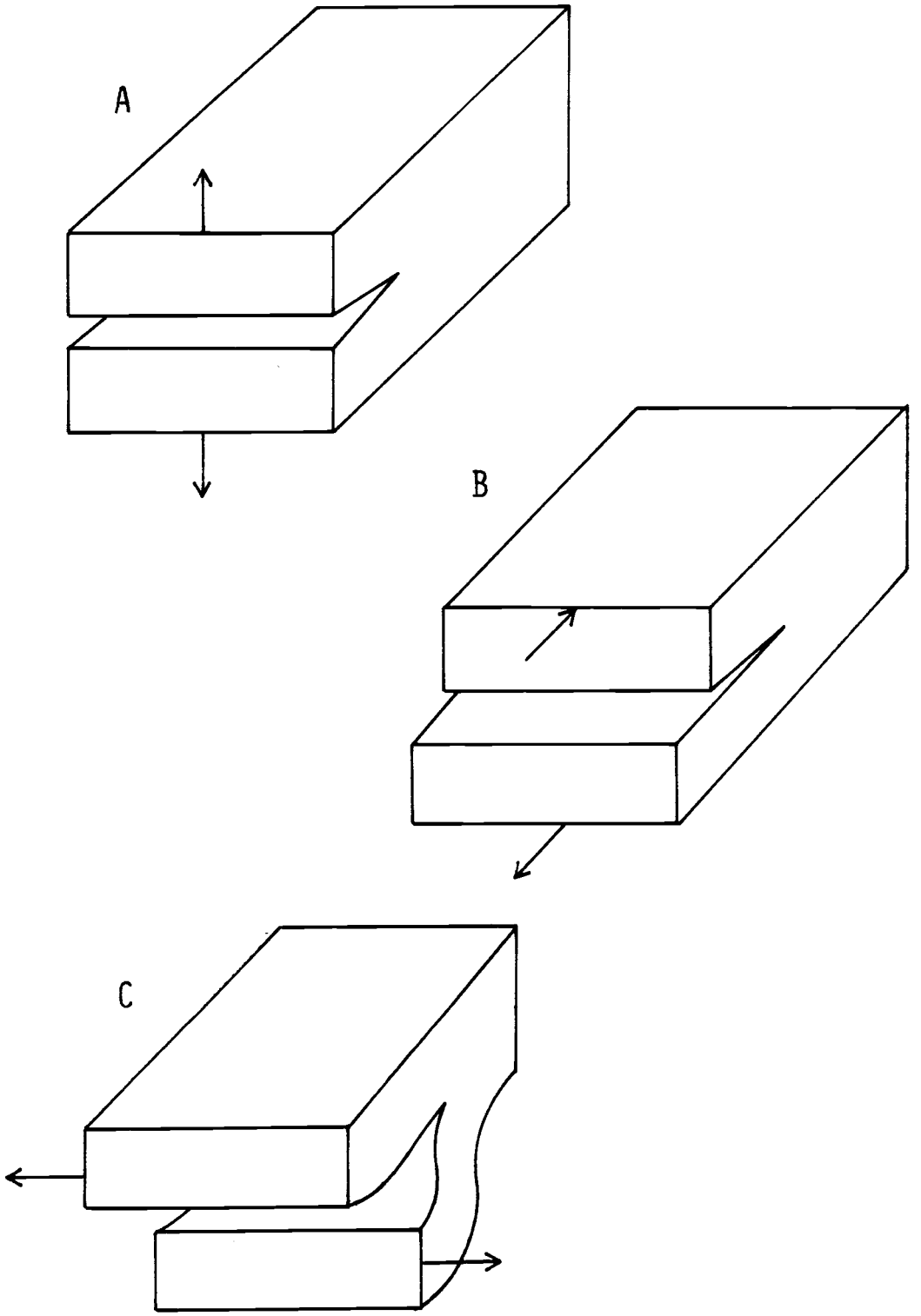

Figure 3. The three modes of brittle fracture: A) opening mode (mode I), B) sliding mode (mode II), C) tearing mode (mode III).

of the crack surfaces tend to separate symmetrically with respect to the initial crack plane.

Mode II: Sliding Mode (Figure 3B). The displacements of the crack surfaces is in the plane of the crack and perpendicular to the leading edge of the crack.

Mode III: Tearing Mode (Figure 3C). The displacements of the crack surfaces are in the plane of the crack and parallel to the leading edge of the crack.

Following Irwin's approach[17], consider a crack loaded in a plate of infinite length, under biaxial stress conditions with the origin of the coordinate system located at the crack tip (Figure 4). Making use of the semi-inverse method of Westergaard[40], Irwin arrived at the following expressions for mode I stresses at the tip of a crack[36].

$$\sigma_x = \frac{K_I}{\sqrt{2\pi r}} \cos\frac{\theta}{2}\left(1 - \sin\frac{\theta}{2}\sin\frac{3\theta}{2}\right)$$

$$\sigma_y = \frac{K_I}{\sqrt{2\pi r}} \cos\frac{\theta}{2}\left(1 + \sin\frac{\theta}{2}\sin\frac{3\theta}{2}\right)$$

$$\tau_{xy} = \frac{K_I}{\sqrt{2\pi r}} \sin\frac{\theta}{2}\cos\frac{\theta}{2}\cos\frac{3\theta}{2} \qquad (7)$$

$$\sigma_z = 0 \quad \text{for plane stress conditions}$$

$$\sigma_z = \nu(\sigma_x + \sigma_y) \quad \text{for plane strain conditons}$$

Similar expressions may be obtained for mode II and mode III cases, although they will not be considered here.

The parameter K_I in these equations is known as the stress

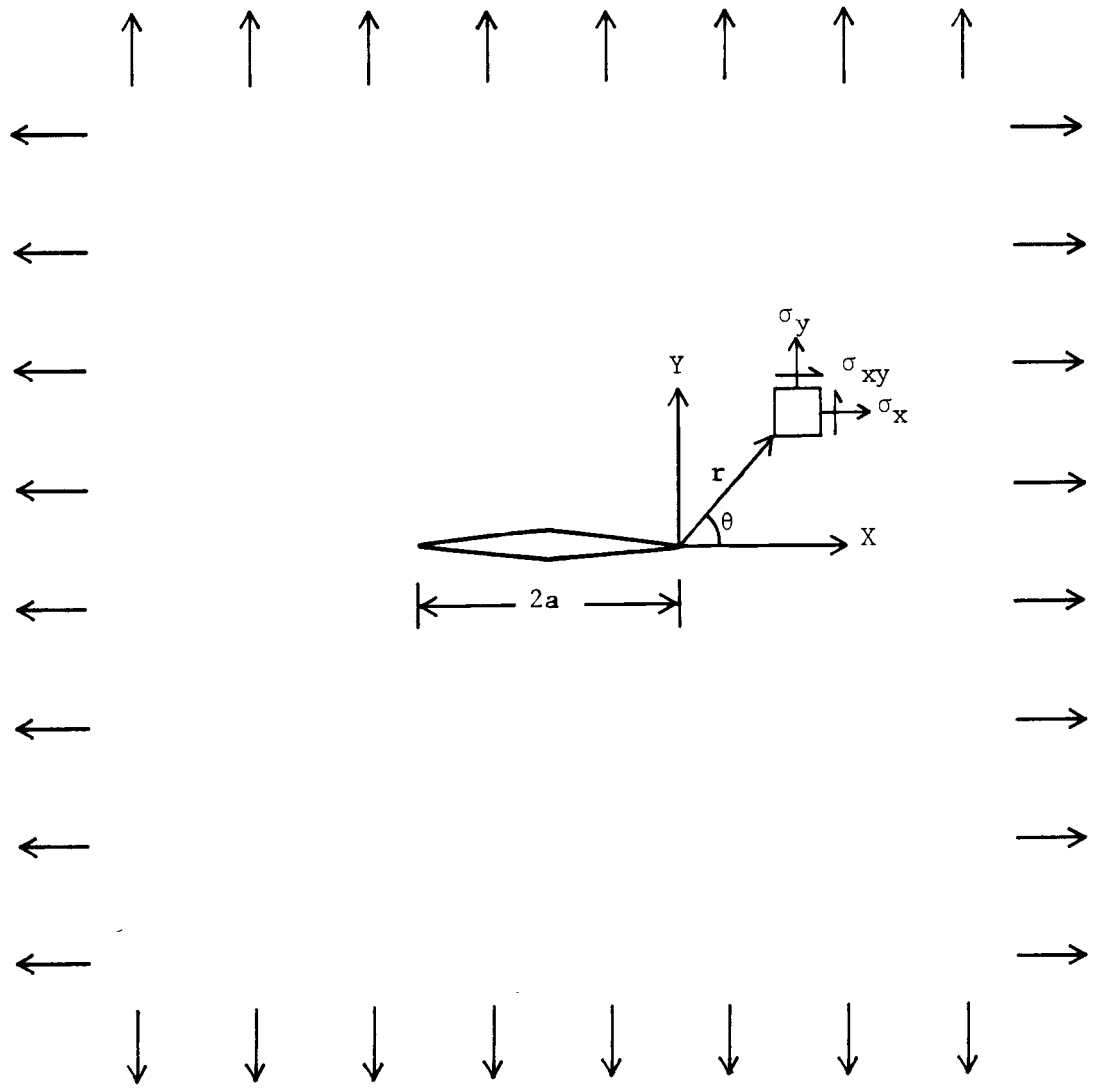

Figure 4. Mode I crack in a plate of infinite length loaded under bi-axial stress.

intensity factor. This may be regarded as the intensity of load that is transmitted through the crack tip region. A physical interpretation of K is given by Tada as representing[36]

> "the intensity of the linear elastic stress distribution surrounding a crack tip, where small amounts of nonlinearity at the crack tip are embedded well within the field and do not significantly disturb it".

With this in mind, since the fracture process is a result of the surrounding crack tip stress distribution, the intensity factors play a large role as fracture parameters in current practice. Different values of K_I, K_{II}, and K_{III} have been obtained for various specimen dimensions, loading conditions, and material types and are available in the literature[36]. For the case of a through-the-thickness center cracked infinite plate loaded under biaxial tension the mode I stress intensity factor is expressed as

$$K_I = \sigma\sqrt{\pi a} \qquad (8)$$

where a is the crack length.

From Equations (6) and (8) it may be shown that for the case of a center cracked infinite plate loaded under biaxial tension the energy release rate, G, may be related to the stress intensity factor, K, as

$$G_I = \frac{K^2}{E} \qquad (9)$$

for plane stress conditions.

Irwin recognized the fact that under most loading conditions materials tend to exhibit small plastic deformations at the crack tip

region[6]. The elastic solutions (Equations 7) allow the stresses to become infinite when the distance from the crack tip, r, approaches zero. In reality this cannot occur and plastic deformations occurring at the crack tip keep the stresses finite.

Irwin argued that the occurrence of plasticity makes the crack behave as if it were longer than its physical size. Due to this crack tip plasticity actual displacements are larger than in the purely elastic case. Irwin suggested that the actual crack length, a, be expressed as an effective crack size, a_{eff}, equal to $a + \delta$, the physical crack size plus a correction δ. The quantity δ is known as Irwin's plastic zone correction. It is normally estimated to be approximately one half the diameter of the actual plastic zone size.

It should be kept in mind that all of the conditions discussed up to this point have dealt with the concepts of linear elastic fracture mechanics. Although the idea of a plastic zone correction factor implies some nonlinear behavior, it is assumed that this takes place on a small scale only. Small scale yielding implies that the size of the plastic zone at the crack tip is small compared to the region in which the elastic crack tip stress field equations apply. In other words, the nonlinear or plastic zone may be regarded as being well embedded in the surrounding elastic region. In the case of large scale yielding or regions of strictly plane stress behavior other elastic-plastic concepts (e.g. J-integral) should be utilized. This leads us to a discussion of plane stress versus plane strain and their importance in the design process.

Plane Stress versus Plane Strain

Plane stress corresponds to a situation when a plate that is loaded parallel to the x-y plane is allowed to deform in the thickness direction (in the z direction). It is a function of specimen thickness and normally occurs in very thin specimens. The mathematical definition of plane stress is

$$\begin{aligned} \sigma_z &= 0 \\ \tau_{xz} &= 0 \\ \tau_{yz} &= 0 \end{aligned} \qquad (10)$$

On the other hand, plane strain corresponds to a similar loading condition but deformation in the thickness direction is restrained. Plane strain conditions normally occur in very thick specimens. The mathematical definition of plane strain is

$$\begin{aligned} \varepsilon_z &= 0 \\ \gamma_{xz} &= 0 \\ \gamma_{yz} &= 0 \end{aligned} \qquad (11)$$

The definitions given here for plane stress and plane strain correspond to conditions of stress or strain throughout the deformed body. In fracture mechanics, however, the meaning of plane stress and plane strain normally refer to the stress and strain conditions at a very localized point in a specimen (e.g. at the tip of a crack). They

indirectly refer to the size of the plastic zone that exists at the tip of a crack under a given loading condition. Small plastic zones refer to plane strain conditions whereas large plastic zones refer to plane stress conditions. As a result, since linear elastic fracture mechanics concepts are based on linear elastic material behavior, the term plane stress versus plane strain takes on very important consequences in the field of linear elastic fracture mechanics. For example, consider a material that behaves in a linear elastic manner. The critical stress intensity factor, K_{Ic}, is known to be constant and is independent of specimen thickness for plane strain conditions. Under these conditions, the plastic zone at the tip of a crack is small and is constrained by the elastic material surrounding it (e.g. small scale yielding). Strains in the thickness direction are zero (e.g. $e_z = 0$) due to the surrounding elastic material (See Figure 5a).

In plane stress conditions, however, where the size of the plastic zone is large, free yielding is allowed to take place in the thickness direction (See Figure 5b). This influences the state of stress within the body. The size of the plastic zone changes as specimen thickness changes. Therefore, K_{Ic} changes as specimen thickness changes. Eventually, for materials that behave in a linear elastic manner, as specimen thickness increases, plane strain conditions prevail (Figure 6).

This condition of plane stress versus plane strain brings up a question as to the validity of K_{Ic} as a practical design criteria. In plane strain conditions K_{Ic} is assumed to be a material constant. Thus, it is very useful in terms of ranking materials according to their toughness. For this reason, standardized tests to determine

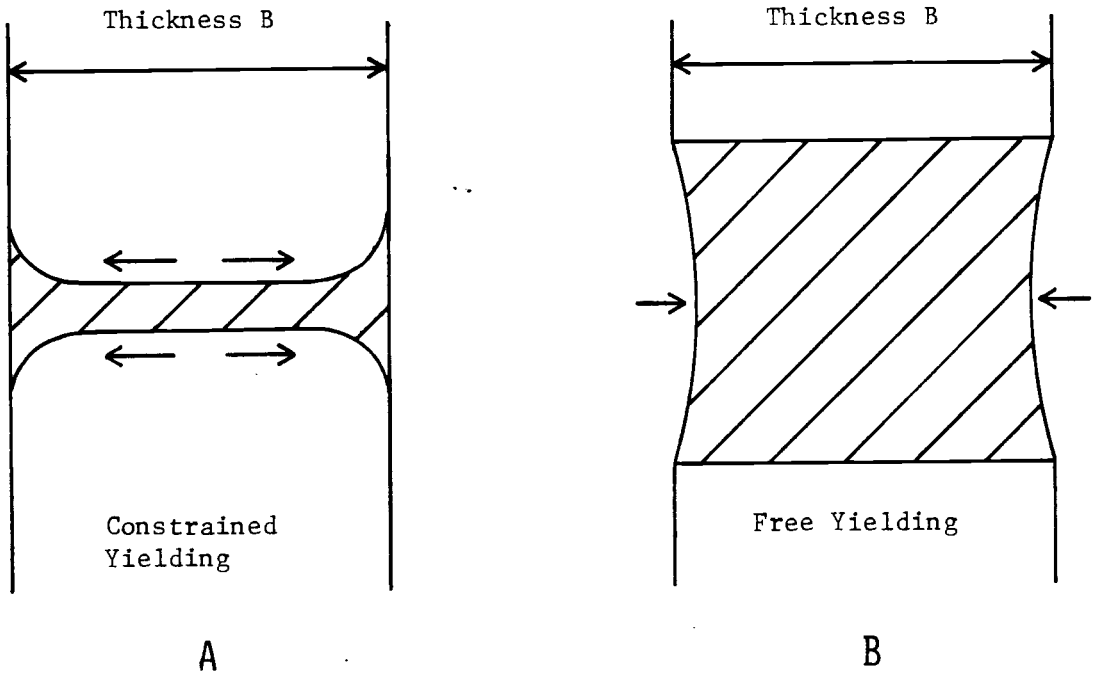

Figure 5. Effect of plastic zone size on specimen yielding.
A) small plastic zone, B) large plastic zone.

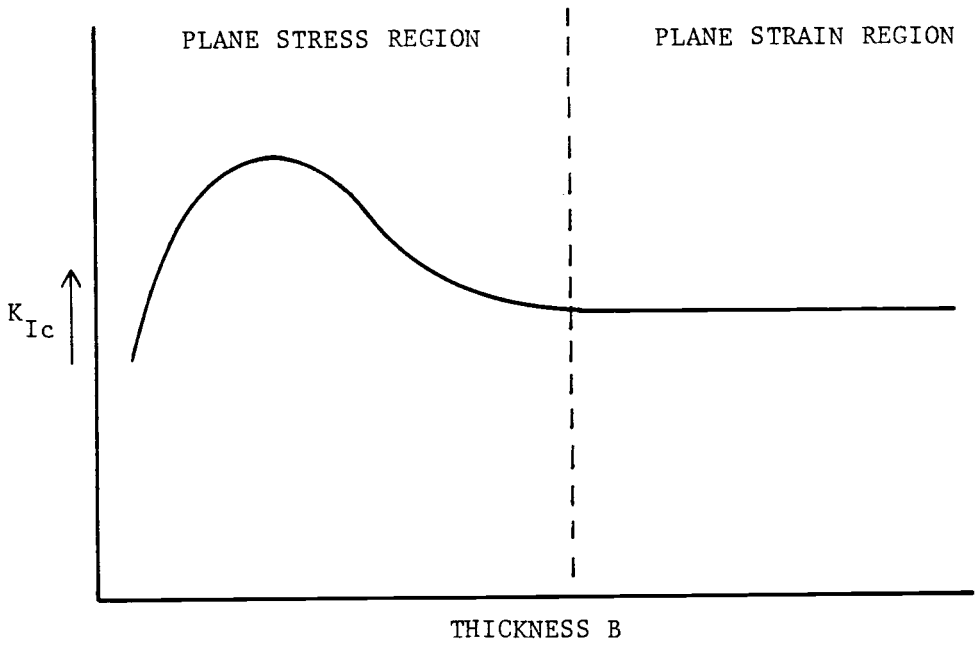

Figure 6. Toughness as a function of thickness.

critical stress intensity factors are normally performed under plane strain conditions. However, because of insufficient thickness, practical structures often exhibit plane stress behavior. In these cases, the actual toughness is usually higher than the measured K_{Ic}, resulting in very conservative design procedures. For design purposes, it should be kept in mind that for each application in which toughness values are to be used, geometry and thickness effects should be considered.

For ductile materials that exhibit properties of high toughness and low yield strength, a high degree of nonlinearity is often observed. This may be due partially to specimen geometry and partially to nonlinear material behavior. To compensate for nonlinear material behavior due to specimen geometry, standardized tests (ASTM E399) for materials that exhibit properties of high toughness and low yield strength require that the specimen thicknesses be very great, sometimes on the order of one meter[6]. Obviously, since this is impractical other fracture mechanics concepts that allow for nonlinear behavior (e.g. J integral) should be used.

Elastic-Plastic Fracture Mechanics - the J Integral Method

When the plastic zone at the tip of a crack is small compared to the crack size the principles of LEFM may be usefully applied. Under such circumstances plane strain conditions prevail and fracture may be characterized by K_{Ic} or G_{Ic}. Even in cases where plane stress prevails but fracture takes place at relatively low stresses in comparison to the yield stress there are satisfactory ways in which LEFM concepts may be used[6]. However, when the size of the plastic zone becomes very

large compared to the crack size, the principles of LEFM no longer apply. This normally is the case in materials the exhibit low yield strength, high toughness properties.

Under these conditions plastic flow at the crack tip is no longer constrained as in the linear elastic case, but is allowed to spread throughout the entire cracked section. This is normally referred to as the case of general yielding. Under these conditions the concepts of elastic-plastic fracture mechanics must be used to characterize fracture toughness.

One of the most common approaches to measuring elastic-plastic fracture toughness is through the use of the so called "J-integral". The J integral, initially proposed by Rice[30, 31], has been used to characterize material fracture toughness including both nonlinear elastic and plastic response. For fully elastic material response, the J integral is identical to the strain energy release rate, G, of a material. Thus, the J integral is often described as a direct extension of linear elastic concepts to include large scale plastic behavior.

Rice first proposed the J integral as a two dimensional energy line integral as

$$J = \int_{\Gamma} \left(W\, dy - T \frac{\partial u}{\partial x}\, ds \right) \qquad (12)$$

where W is the strain energy per unit volume, Γ is the path of integration followed counterclockwise in a stressed solid, and T is the outward traction vector on ds (Figure 7A). Rice proved that the J integral is path independent (e.g. J = 0) around any closed contour such as ABCDEF in Figure 7B[30, 31]. This can be shown by noting that

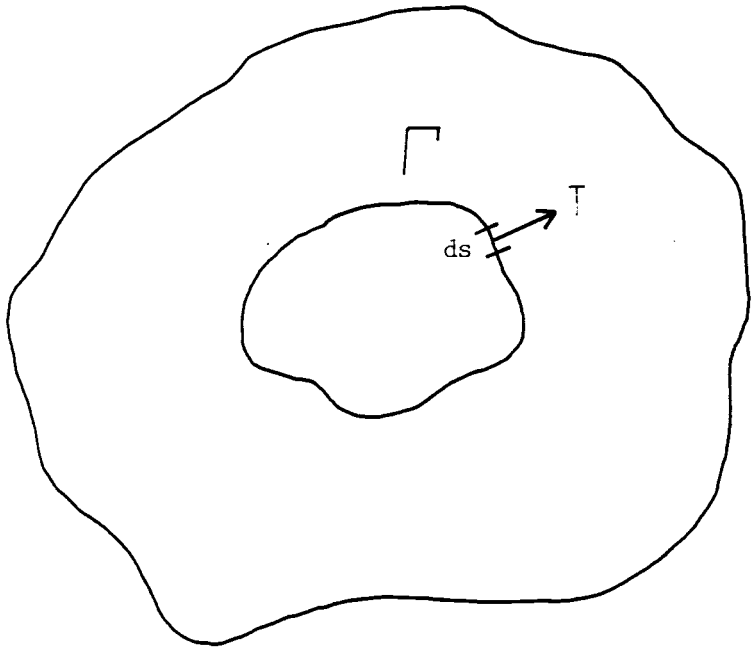

Figure 7a. Definition of the J integral.

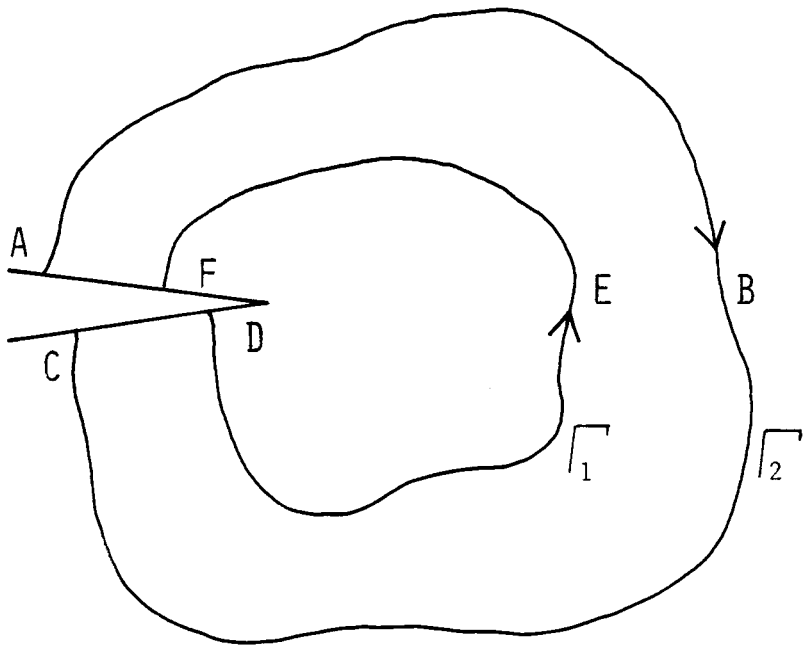

Figure 7b. Contour around a crack tip.

T = 0 and dy = 0 along CD and AF in Figure 7B. The contribution of ABC must be equal and opposite to the contribution of DEF; thus proving path independence.

A more simplistic, physical way of representing J is by an energy rate interpretation similar to Griffith's linear elastic approach, where

$$J = -\frac{1}{B}\frac{\partial U}{\partial a}\Big|_{\Delta = \text{const.}} \qquad (13)$$

and a is the crack length, U is the potential energy, B is the specimen width (assumed to be constant), and Δ is the applied constant load point displacement. It has been shown that J is independent of the loading conditions (e.g. fixed displacement, Δ or constant load, P) due to a second order differential in the energy which may be neglected[19].

This energy rate interpretation is the method used for experimentally determining J. For fully elastic cases, Equation 13 represents a general measure of a materials' fracture toughness because no assumptions concerning material behavior (linear or nonlinear) are made. The energy required for crack extension, U, is simply the area under the load-deflection curve. U may be experimentally measured as the change in area under the load deflection curve as the crack extends a distance (a) to (a + da).

For the linear elastic case, J may be described as the crack driving force. For nonlinear elastic material response J may be interpreted as the energy available for crack extension. However, for the case of plastic behavior where deformation is not reversible, J loses its physical significance as a crack driving force. For elastic-

plastic materials J is a measure of the characteristic crack tip elastic-plastic field[3]. In other words, in the elastic-plastic case, J may be thought of as a measure of the energy required for crack extension which includes some work that causes plastic deformation.

Consider the load deflection curves of three different types of materials; one linear elastic, the next nonlinear elastic, and the third elastic-plastic. Figure 8a shows the load deflection curves of these materials before any crack extension takes place. The linear and nonlinear material response is the same in loading as in unloading. However, the elastic plastic material does not respond in the same manner in unloading as in loading. This area under the load deflection curve in the elastic-plastic case is strictly the work required to cause a plastic or permanent deformation in that material.

Now consider the same three materials after crack extension takes place (Figure 8b). The energy in the shaded area in the linear elastic and nonlinear elastic cases is the energy required to extend the crack a distance (a) to (a + da). For the elastic-plastic case, however, the shaded area is the energy required for crack extension plus work required to cause plastic deformation. This is why, in the elastic plastic case J is referred to as being a measure of the characteristic crack tip elastic plastic field[3].

The J integral method is the most general method that currently exists for determining fracture toughness. However, it does have its limitations. The J integral elastic-plastic approach is based on the so called "deformation theory of plasticity"[20]. The deformation theory of plasticity is in essence identical to a material behaving in a nonlinear elastic sense as long as unloading does not occur. Because

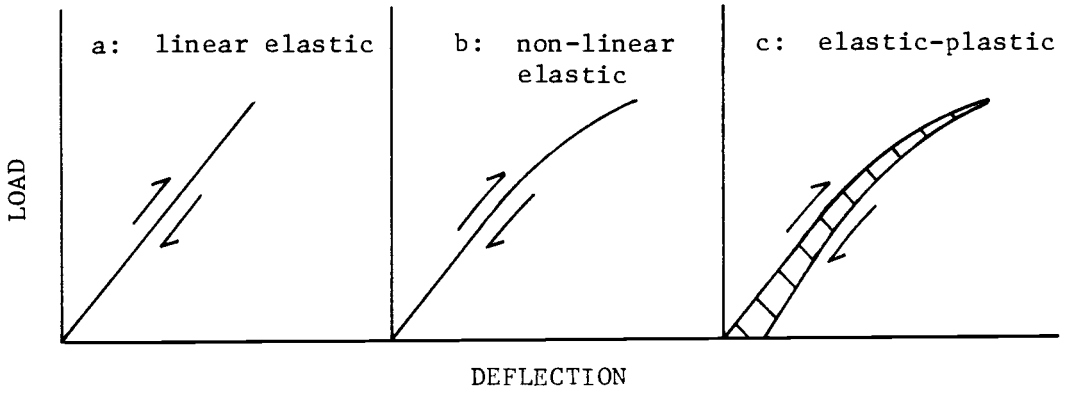

Figure 8a. Load versus deflection curves for three materials before crack extension. In the linear elastic and nonlinear elastic cases the load-unload curves are the same. In the elastic-plastic case the shaded area is the work required to cause plastic deformation.

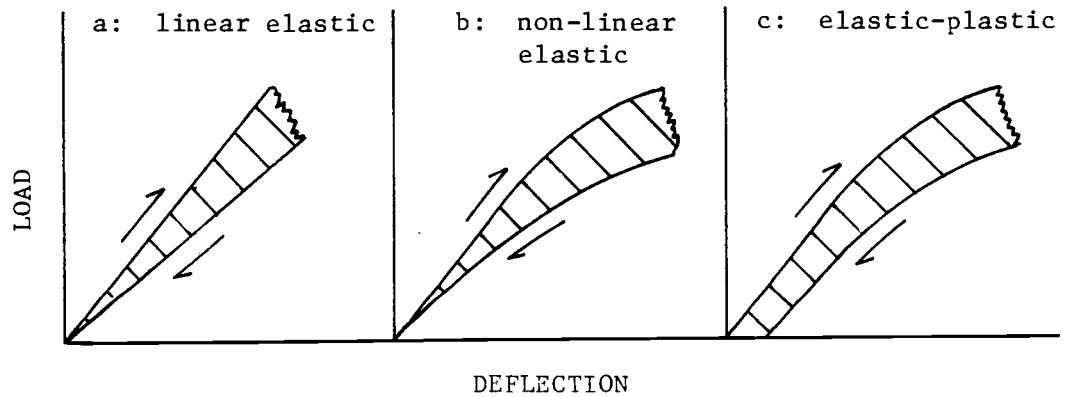

Figure 8b. Load versus deflection curves for three materials after crack extension. In the linear elastic and nonlinear elastic cases the shaded area is the energy required for crack extension. In the elastic-plastic case the shaded area is the energy required for crack extension plus work of plastic deformation.

plastic deformation is not reversible, the use of the J integral approach is restricted to monotonic loading only. Unloading is not permitted. For example, under elastic-plastic conditions, J may be determined from the difference in areas of load deflection curves for identical specimens with varying crack lengths, provided the specimens have never undergone any past loading histories.

Assume a J_{Ic} value has been determined for an elastic-plastic material using specimens that have never been stressed. Then a value is determined using specimens of the same material that have undergone some sort of past loading history. These two J_{Ic} values, although for identical materials, may not be the same. It has not been shown that loading a cracked body and then extending the crack under load will give the same load-deflection curve as initially extending the crack and then loading. Past loading history is a very important concept in elastic-plastic material behavior and must be recognized before any analysis procedures can be correctly performed.

To get a physical interpretation of the elastic-plastic fracture process consider the model described by Matthews and West[24] shown in Figure 9. As the material containing a sharp crack is loaded the crack tip becomes blunted. This blunting increases as the load is increased causing plasticity to set in. Finally, a load is reached where a crack advance occurs ahead of the original blunted crack. Fracture toughness is measured at the point where this crack advance occurs. This point is labeled J_{Ic}.

The test method for determining a single J value described by Landes and Begley[19, 20] is shown in Figure 10. Using this method, several specimens of varying crack lengths are tested. Load is applied

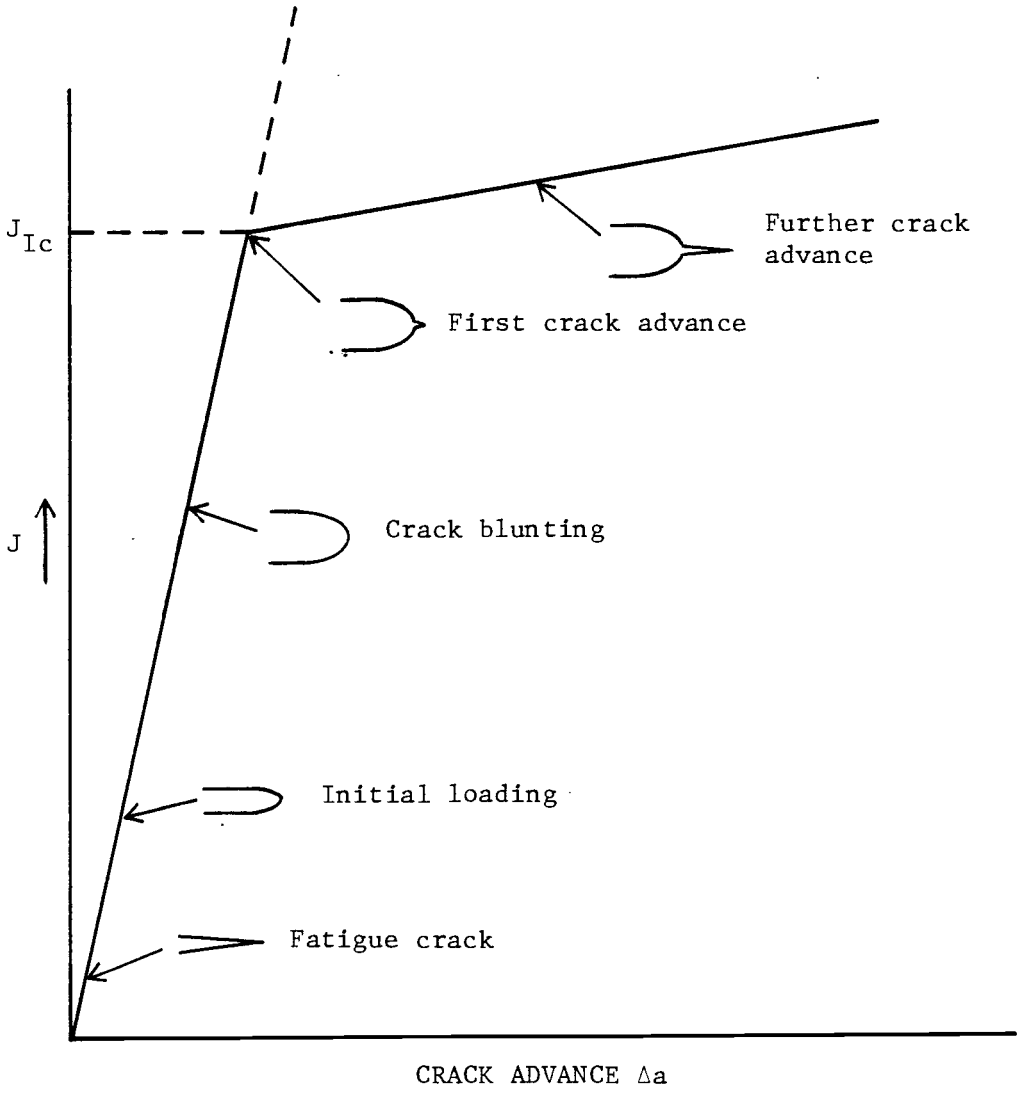

Figure 9. Physical interpretation of the elastic-plastic process showing point of J_{Ic}.

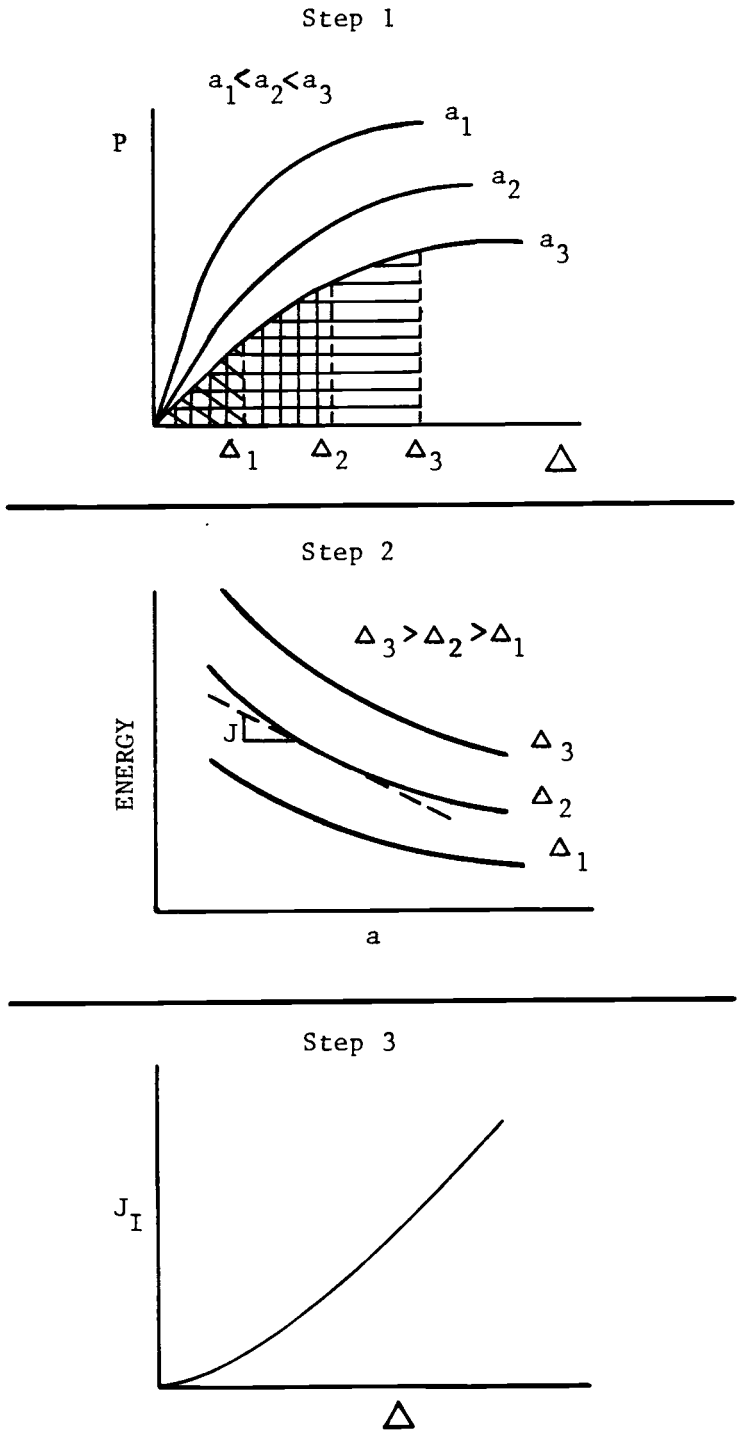

Figure 10. Energy rate determination of J.

in a specimen with crack length, a, until the crack extends, where a curve of load versus load point displacement is measured. This procedure is repeated for the next specimen with crack length (a + da), and so on until a representative number of specimens with varying crack lengths are tested. The energy under each of these curves can be plotted as a function of crack length for various constant displacements. The slopes of these curves are then defined as J. Curves of J versus displacement for various crack lengths may then be constructed. The maximum displacement at which crack extension occurred for a given specimen may then be used to determine the value of the critical failure energy, J_{Ic}.

Experimental Methods for Determining Fracture Toughness Parameters

General Procedures

Up until this point the general concepts of fracture mechanics have been presented with emphasis on the effects of various material behavior on fracture toughness parameters. The remainder of this report will be directed toward experimental methods of determining mode I fracture toughness parameters. The interlaminar failure of composite materials is of foremost importance.

The procedure for plane strain fracture toughness for metallic materials is standardized by the American Society for Testing and Materials. ASTM E 399[1] provides the geometrical requirements that plane strain conditions will exist at a crack tip during a mechanical tensile test. The necessity for plane strain conditions for the evaluation of K_{Ic} have already been discussed elsewhere in this report. Presently, there exists only standardized tests for determining mode I stress intensity factors. Various geometrical loading configurations for determining plane stress and plane strain, mode II and mode III stress intensity factors are available in the literature[36].

Two men responsible for the development of ASTM E 399 were Srawley and Brown[7, 35]. Through extensive testing and analysis with metallic materials they arrived at three recommended specimens to be used in the determination of the mode I stress intensity factor, K_{Ic}. They are the three-point bend specimen, the compact tension specimen, and the C-shaped specimen. The three-point bend and compact tension specimens are the general purpose specimens whereas the C-shaped specimen was primarily designed for testing of cylinders and thick bars. All

specimens, however, yield comparable results.

Composite Interlaminar Fracture Toughness

When applying fracture mechanics to laminated composite materials complications often arise due to the fact that the use of the stress intensity factor equations (Equations 7) require complex analysis methods to determine stress distributions at the crack tip. For this reason design analysis is often based on the strain energy release rate, G, rather than the stress intensity factor. The strain energy release rate may be experimentally measured using specimens that do not require complex analysis methods.

Normally, the specimens suggested by ASTM E 399 are not suitable for interlaminar fracture characterization of composite materials. Fabrication of such specimens having geometrical dimensions required by ASTM E 399 would be very costly and unrealistic.

There are a number of specimens which have been proposed for evaluating interlaminar strain energy release rates in composites[9, 18, 32, 33, 38, 41, 42]. Among these are the edge delamination specimen[32], the center cracked tension specimen[42], the surface notched specimen[38], and the lap shear specimen[41] (Figure 11). These specimens, however, develop complex stresses at the crack tip which require finite element analysis methods to determine fracture toughness parameters.

One specimen which has been successfully used to characterize interlaminar fracture of composites has been the double cantilever beam (DCB) specimen shown in Figure 11E. The DCB specimen has been known to yield slow stable crack extension and has the advantage that the same

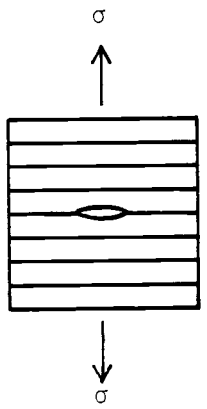

A) Center Cracked Specimen

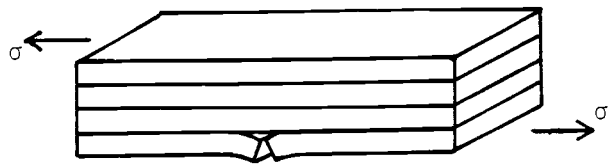

B) Surface Notched Specimen

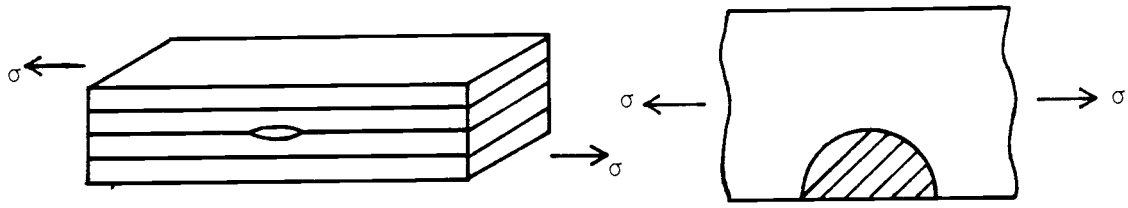

C) Edge Delamination Specimen

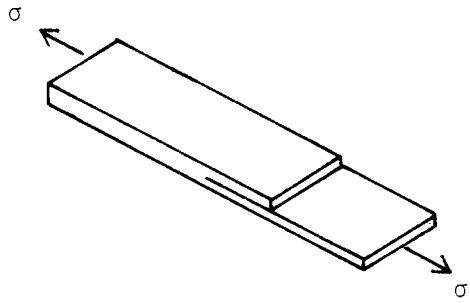

D) Lap Shear Specimen

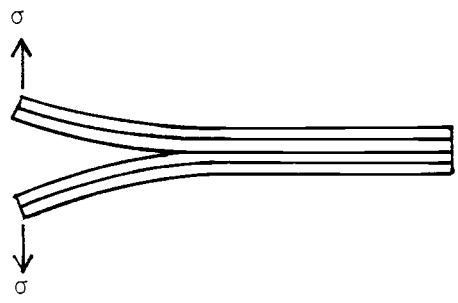

E) Double Cantilever Beam

Figure 11. Typical composite interlaminar fracture toughness specimens.

specimen may be used to collect a large amount of data points. It also requires less extensive analysis methods to determine fracture toughness parameters than the other specimens previously mentioned. For this reason, the DCB specimen was chosen for this study to characterize fracture toughness parameters.

The use of the DCB specimen as a qualitative measure of fracture toughness for metals and adhesives has been prevalent for a number of years[14,26]. It has also been known to have a considerable amount of success in characterizing fracture toughness parameters in composite materials[11,33,44]. The critical strain energy release rate, G_{Ic}, is defined as

$$G_{Ic} = -\frac{1}{B}\frac{\partial W}{\partial a}\Big|_{\Delta = \text{const.}} \qquad (14)$$

where $\frac{\partial W}{\partial a}$ is the crack driving force per unit thickness, B. Various expressions for G_{Ic} may be obtained from Equation 14 by making certain assumptions about material behavior. For example, if we assume linear elastic behavior the work term, W, in Equation 14 (which is the energy required to cause crack extension) will take the form

$$W = \frac{P_{max}\,\Delta}{2} \qquad (15)$$

where P_{max} is the critical load at which crack extension takes place, and Δ is the applied load point displacement for a given crack length. The compliance of a specimen for a characteristic crack length is the reciprocal slope of the P-Δ curve and is defined as

$$c = \frac{\Delta}{P} \qquad (16)$$

Substituting Equations 15 & 16 into Equation 14 an expression for G_{Ic} may be obtained as

$$G_{Ic} = \frac{P_{max}^2}{2B} \frac{dc}{da} \qquad (17)$$

Equation 17 is a very useful expression for materials that exhibit linear elastic behavior because it may be easily obtained experimentally in the absence of a complex mathematical analysis. Expressions for c=f(a) may be found experimentally by performing a number of tests over a wide range of crack sizes. The derivative in Equation 17 follows from numerical calculations. Again, an advantage of the DCB specimen is that the same specimen may be used for a number of crack lengths to determine the c versus a curve.

To further simplify Equation 17, one may assume the material to be an isotropic linear elastic material (e.g. constant E) that follows simple beam bending theory (neglecting large deflections and rotations). The load point displacement at crack extension may be calculated as

$$\Delta = \frac{2P_{max}\, a^3}{3EI} = \frac{8P_{max}\, a^3}{E\, h^3\, B} \qquad (18)$$

where E is the Youngs Modulus, h is 1/2 the total uncracked specimen thickness, B is the specimen width, P_{max} is the load at which crack extension occurs and a is the crack length before extension. From this expression the compliance may be determined as

$$c = \frac{\Delta}{P} = \frac{8\, a^3}{E\, h^3\, B} \qquad (19)$$

and similarly the critical energy release rate is given by

$$G_{Ic} = \frac{P_{max}^2}{2B}\frac{dc}{da} = \frac{12\ P_{max}^2\ a^2}{E\ h^3\ B^2} \qquad (20)$$

This expression assumes that the presence of nonlinear effects due to large deflections and rotations are small and may be neglected. For thin composite DCB testing it may be necessary to consider nonlinear effects of large deflections and rotations which may be present. Normally, these nonlinear effects are very small in conventional DCB testing of metallic specimens but, because of the low flexural rigidity of thin composites, effects due to large deflections and rotations may be present and should be accounted for in the analysis. Devitt[11] studied this problem using a correction to the linear theory made by Bisshopp and Drucker[5], in which elliptic integrals were used in the analytic solution to compensate for nonlinear effects. Devitt found that nonlinear effects were significant when

$$\frac{\Delta}{2a} > 0.40 \qquad (21)$$

as shown in Figure 12. Experimental tests performed on composite specimens with various thicknesses at a number of crack lengths confirmed his analytical results.

It is important to emphasize the assumptions made in deriving the various expressions for G_{Ic}. Although they were all derived from the same basic equation (Equation 14), they each have their own assumptions concerning material behavior which must be strictly adhered to. The

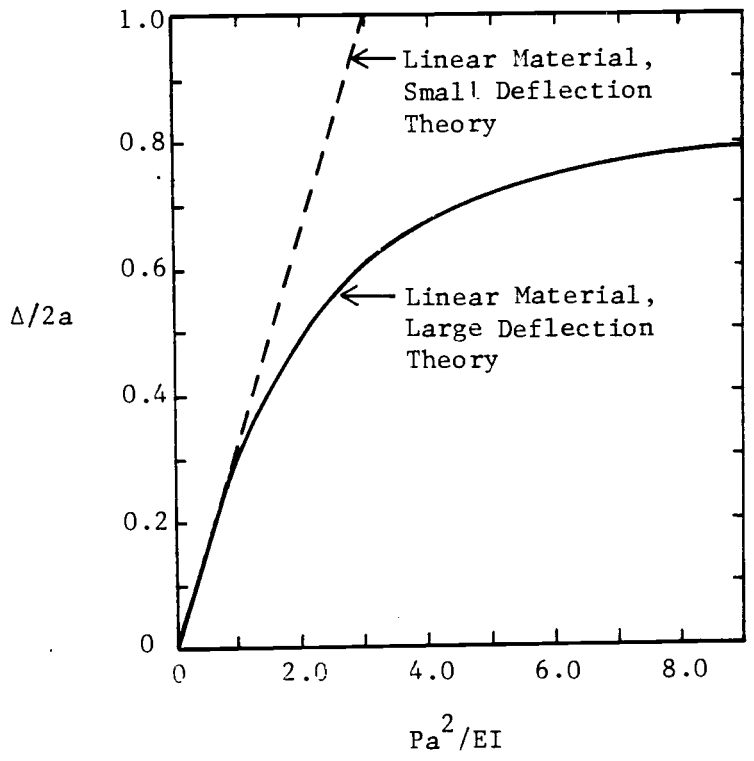

Figure 12. Tip deflections for a uniform cantilever beam as described by Bisshopp and Drucker (5).

compliance calibrated approach for measuring G_{Ic} (Equation 17) assumes linear elastic material behavior but allows the specimen to behave isotropically or anisotropically. Equation 20 assumes that the material be isotropic, linear elastic and that large deflections and rotations are negligible. If the material does not behave according to the assumptions used in deriving a particular equation then that equation should not be used to calculate G_{Ic}. Instead, one must use methods which utilize the original definition of G_{Ic} (Equation 14) such as the J-integral approach.

Analytical Procedure

One of the major objectives of this program was to compare various approaches of measuring fracture toughness data in laminated composite materials. Much of the literature review has focused on the importance of recognizing the type of material behavior specimens exhibit when experimentally tested to evaluate G_{Ic} or J_{Ic}. This material behavior (e.g. linear elastic, elastic plastic ... etc.) plays an important role in determining which analysis method should be used to most accurately describe critical failure energy.

In this program, three analysis methods are used to calculate composite interlaminar fracture toughness data. Each method described below is based on a double cantilever beam specimen. Assumptions relating to material behavior and specimen geometry are presented in the derivation of each method.

Linear Elastic Strain Energy Release Rate

The linear analysis of Equations 18 through 20 assume isotropic linear elastic material behavior. The critical strain energy release rate obtained with this approach will be referred to as the linear G_{Ic} for the remainder of the text. The method of Devitt[11] considered nonlinearity that exists due to large beam deflection. The nonlinear analysis was found to be unnecessary in this study since crack lengths were chosen to be short enough to avoid large deflection effects. For a graphical illustration of the linear method see Figure 13.

Equations 18 and 20 may be combined to remove E from the expression for the linear G_{Ic} to obtain

$$G_{Ic} = \frac{3P_{max}\,\Delta}{2Ba} \qquad (22)$$

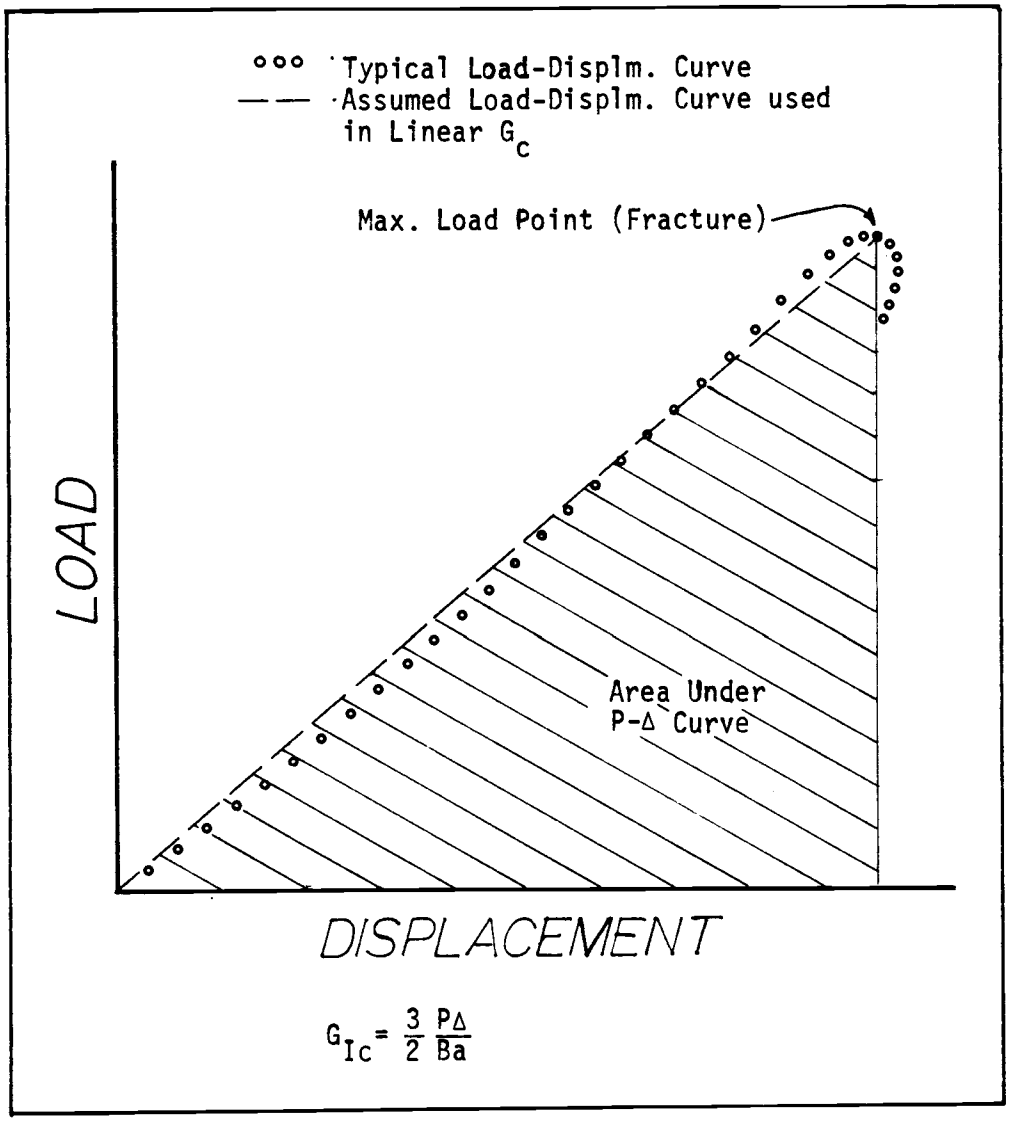

Figure 13. A typical load versus displacement curve showing how the linear G_{Ic} approach treats the experimental data.

Using the expression above for calculating G_{Ic} assumes that information of P_{max} and Δ at a given crack-length is sufficient to determine the behavior of the material for an incremental change in crack length. Thus, the load-displacement response of the material must be well modeled by the elementary beam bending assumptions of the analysis. Simply having a linear load-displacement curve is a necessary but not sufficient condition that the model is adequate.

Compliance Calibrated Strain Energy Release Rate

Direct experimental calculation of G_{Ic} using Equation 17 will be referred to as the compliance calibrated G_{Ic} for the remainder of the text. The compliance calibrated G_{Ic} assumes linear elastic material behavior. Unlike the linear G_{Ic} method, the compliance calibrated G_{Ic} makes no assumptions concerning material response (isotropy) or crack-tip support conditions (cantilever). Instead it uses experimental data to determine anisotropic effects and support conditions. Figure 14 illustrates the compliance calibrated approach. The compliance calibrated G_{Ic} rewritten for convenience is

$$G_{Ic} = \frac{P_{max}^2}{2B} \frac{dc}{da} \tag{17}$$

where P_{max} refers to the maximum load at the onset of crack propagation, B is the specimen width, a is the crack length and c is the compliance. To find $\frac{dc}{da}$ a polynomial fit of differing orders of actual compliance versus crack length test data is used. For all specimens the compliance was measured on the lower 1/4 of the load displacement curves.

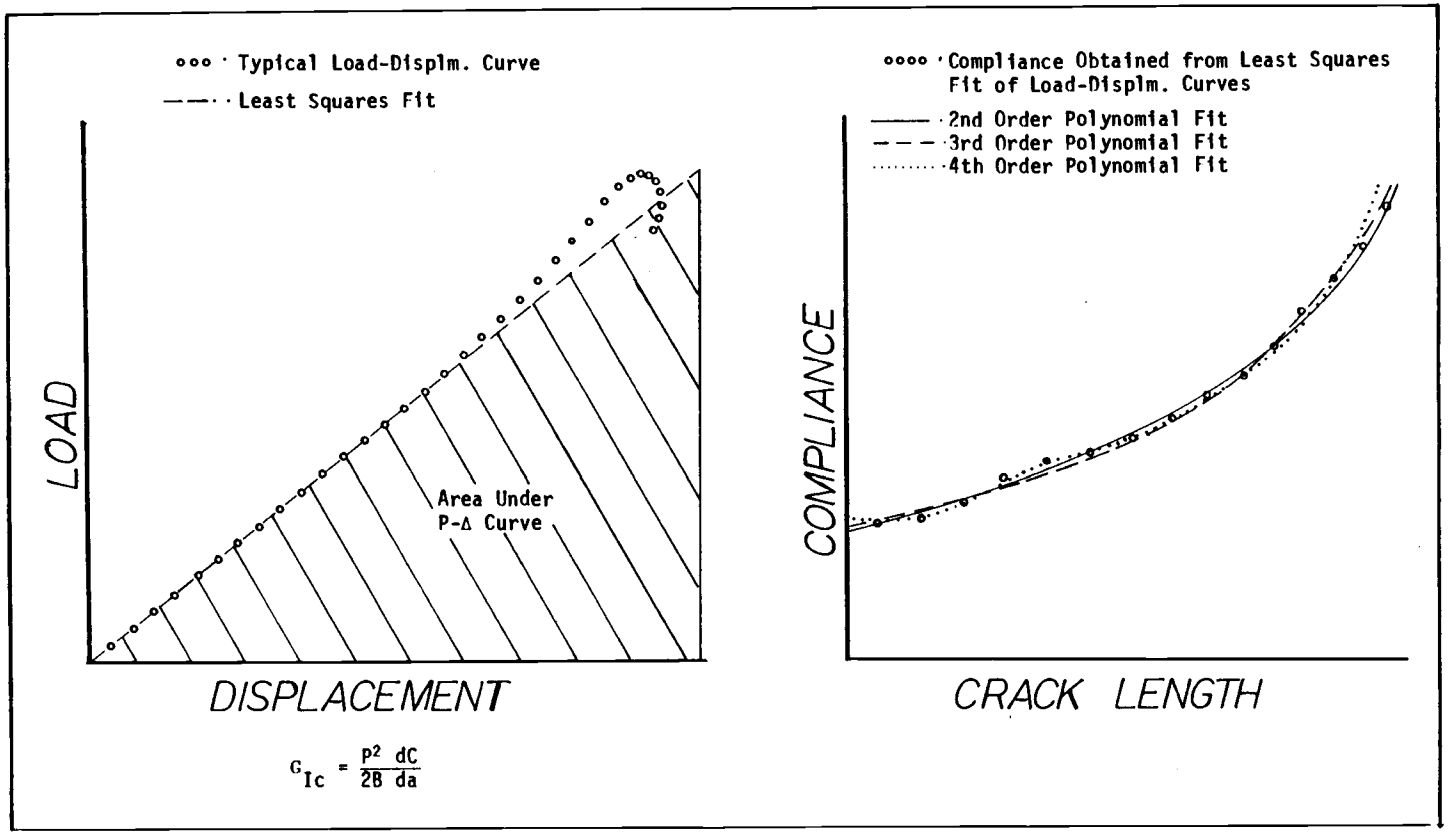

Figure 14. Schematic of the compliance calibrated G_{Ic} approach. Using this approach a linear load versus displacement response is assumed.

Elastic-Plastic J Integral Approach

The J Integral approach, rewritten here for convenience, calculates failure energy directly from the definition;

$$J = -\frac{1}{B} \frac{\partial U}{\partial a} \Big|_{\Delta = \text{const.}} \qquad (13)$$

No assumptions are made as to the nature of the energy required, U, to cause crack extension. The material is allowed to behave in a linear elastic, nonlinear elastic or elastic-plastic manner. This most general method is shown in Figure 15. The total area under each load versus load-point displacement curve at a given value of displacement may be plotted versus crack length. This is performed at a number of displacements to get a number of different energy-crack length curves. Energy versus crack length curves (e.g. energy curves) are then plotted for each displacement. These energy versus crack length curves are constructed using 2nd and 3rd order polynomial fits. After examination of a number of energy curves and their corresponding data points from a number of specimens the polynomial fit that best represents the data may be chosen. The slopes of these energy curves are then defined as $\frac{\partial U}{\partial a}$.

It is often useful for design purposes to construct a J versus displacement curve (e.g. J curve) for various crack lengths. This may be performed by taking the slopes of each energy curve at a given crack length and plotting J curves from the definition of J_I (Equation 13). J_{Ic} is the energy required to cause crack extension. It may be determined as the point at which maximum displacement, Δ, occurred at a given crack length as shown in Figure 16.

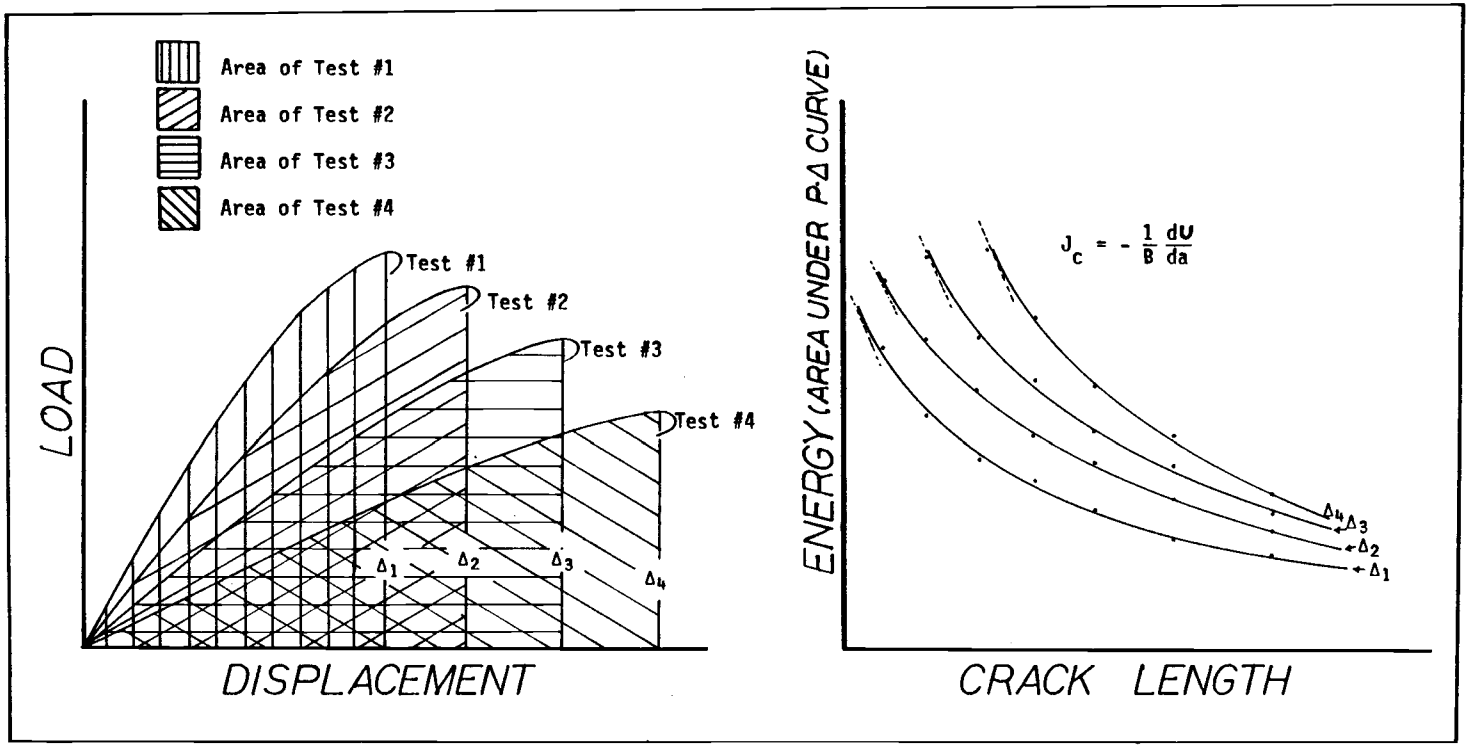

Figure 15. The linear elastic or elastic plastic J integral approach. The method for determining J_{Ic} plots the total area under each load-displacement curve versus crack length. This is performed at a number of displacements to obtain a number of energy versus crack length curves. The critical value may be taken at the tips of the curves as shown in the right-hand figure.

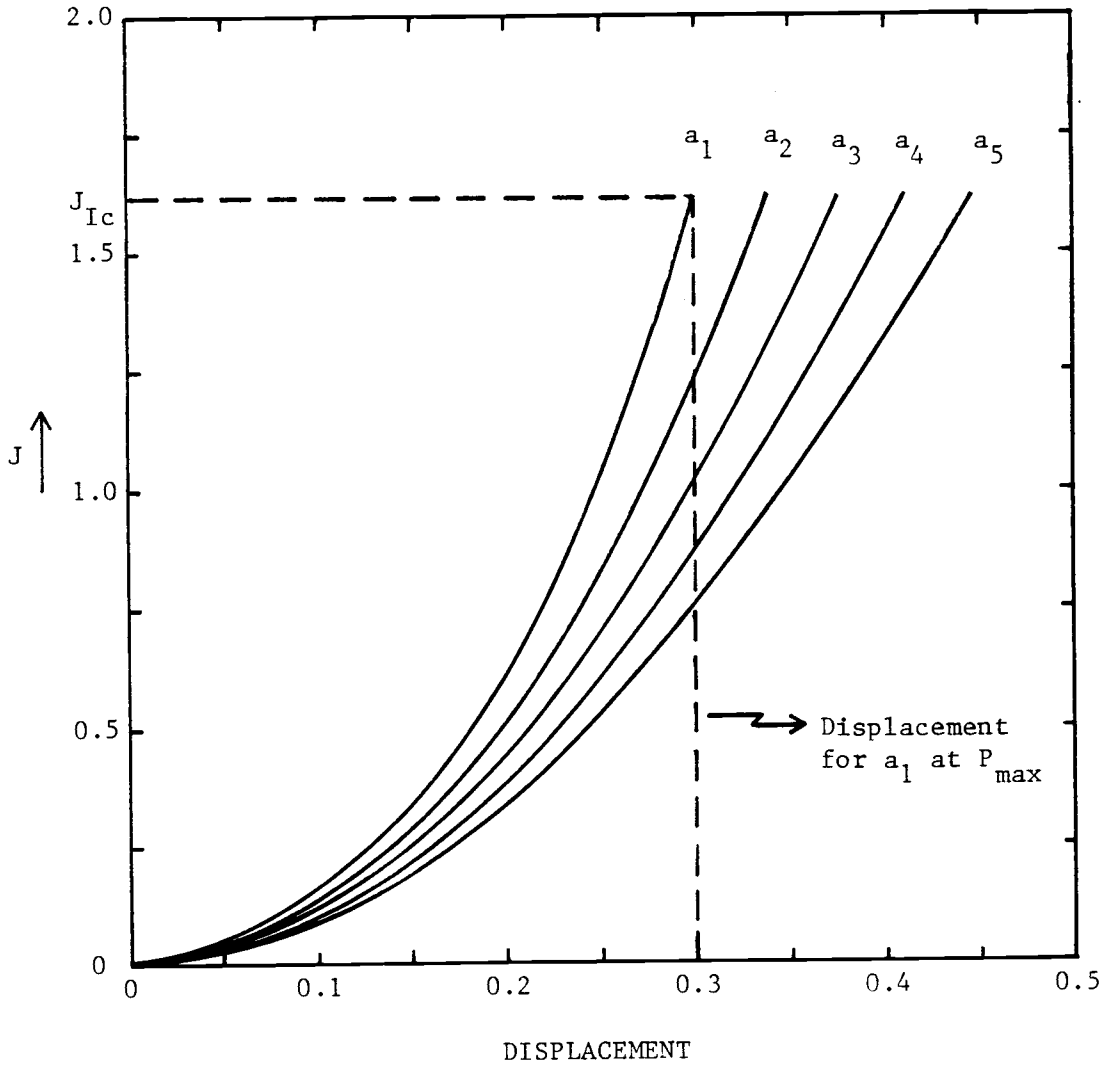

Figure 16. Typical J curves for various crack lengths showing point of J_{Ic} for crack length a_1.

Experimental Procedure

The goal of the experimental portion of this program was to examine the interlaminar fracture behavior of various graphite/epoxy laminated composites and to determine which analysis method would most accurately describe this type of materials fracture toughness strength. A total of three different types of resin systems which comprise the matrix in the graphite/epoxy composite were examined. These resin systems were modified slightly with various types of filler materials. All specimens were the double cantilever beam type with a constant width of 0.50 inches and a length of 11.0 inches. Figure 17 shows a complete description of the test matrix. All specimens examined in this study were 12 plies with each ply approximately 0.0064 inches thick. The effect of specimen thickness on DCB testing will be addressed in the discussion of results section of this report.

Specimen Fabrication

All fabrication of panels consisting of unidirectional tape of graphite fiber in a matrix of epoxy resin was performed at the Boeing Company. The fabrication process consisted of laying up twelve plies of prepeg tape with all plies in the 0^{o} direction. The prepeg tape was provided to the Boeing Company by each individual manufacturer (e.g. Hexcel and American Cyanamid). A thin piece of teflon acting as a crack starter was placed between the 6th and 7th ply at one end approximately 2.5 inches into the panel. The panels were subsequently cured in an autoclave oven under a high temperature and high pressure environment. This curing process, performed under manufacturing specifications, is shown in Figure 18.

RESIN TYPE - SPECIMEN TYPE - SPECIMEN NUMBER

(e.g. BP907 - TYPE A - 3)

RESIN TYPE DESIGNATOR	SPECIMEN TYPE DESIGNATION	NUMBER OF SAMPLES
AMERICAN CYANIMID BP907	A	3
	B	3
	C	3
	D	3
	E	3
	F	3
	G	3
	H	3
	I	3
	J	3
	K	3
	L	3
	M	3
AMERICAN CYANIMID 985	A	3
	B	3
	C	3
	D	3
	E	3
	F	3
	G	3
	H	3
	I	3
	J	3
	K	3
	L	3
HEXCEL F263	A	3
	B	3
	C	3
	D	3
	E	3

Figure 17. Mode I material test matrix. This table shows a complete description of material type, specimen type, and number of specimens tested. All type A specimens were baseline specimens (e.g. no resin modifications). Other types shown contained various resin modifications. The top of the table shows the specimen designations.

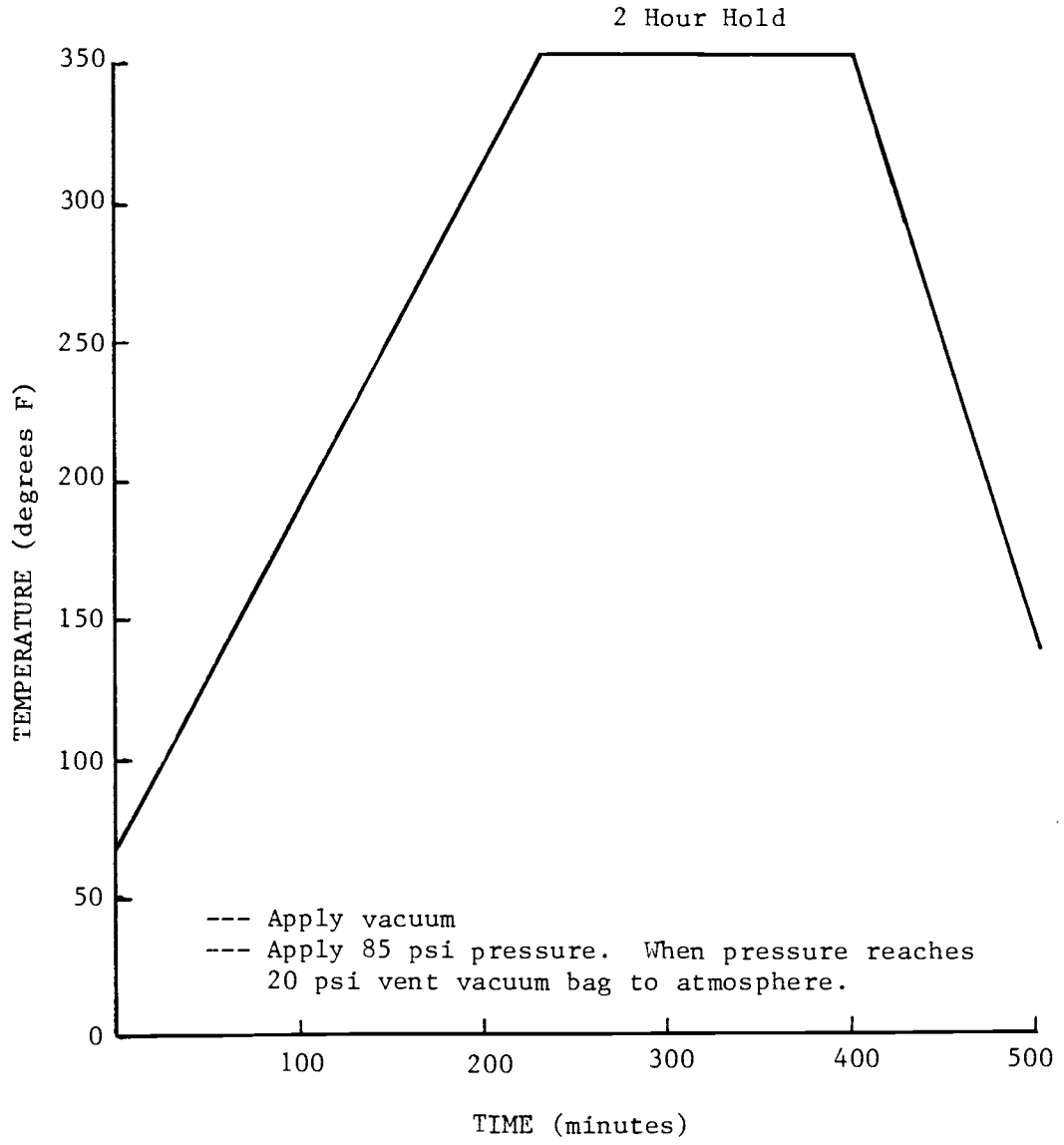

Figure 18. Typical laminate curing cycle.

After curing the panels all edges were trimmed and three specimens from each panel were cut and machined to required dimensions of 0.5" x 11.0" as shown in Figure 19. The specimens were machined such that 1.5 inches of the portion of the specimen containing the teflon film was left to act as a crack starter. The specimens were then sent to Oregon State University where all DCB testing was performed.

Prior to testing, small aluminum adherends, 0.5" x 0.5" x 0.5" were glued to the teflon cracked end of each specimen using hot melt glue. There were used as loading grip attachments. Also, the edges of each specimen were coated with a brittle white liquid paint (white out) to enable the technician to located the position of the crack front during a mechanical test. The final test specimen, in the loaded position is shown in Figure 20.

Test Apparatus

In all testing the following equipment is common:

(1) An INSTRON model TT-B constant displacement testing machine (with associated load cells, drive gears, etc.)

(2) A HEWLETT-PACKARD model 9825 mini-computer (with associated peripheral devices-9862A plotter, several ROM modules, line printer and expanded memory)

(3) A HEWLETT-PACKARD model 3490A digital voltmeter with a programmable GPIB interface to the 9825

(4) A LEEDS AND NORTHRUP model 2740 scanner programmable with a sixteen bit binary interface

(5) Two Schaevitz model 1000 HR-DC LVDT's (linear voltage-displacement transducers)

The goal of the test design for each mechanical test was to provide the maximum amount of data collection possible, to store all data in an easily accessible form, and to provide most or all data

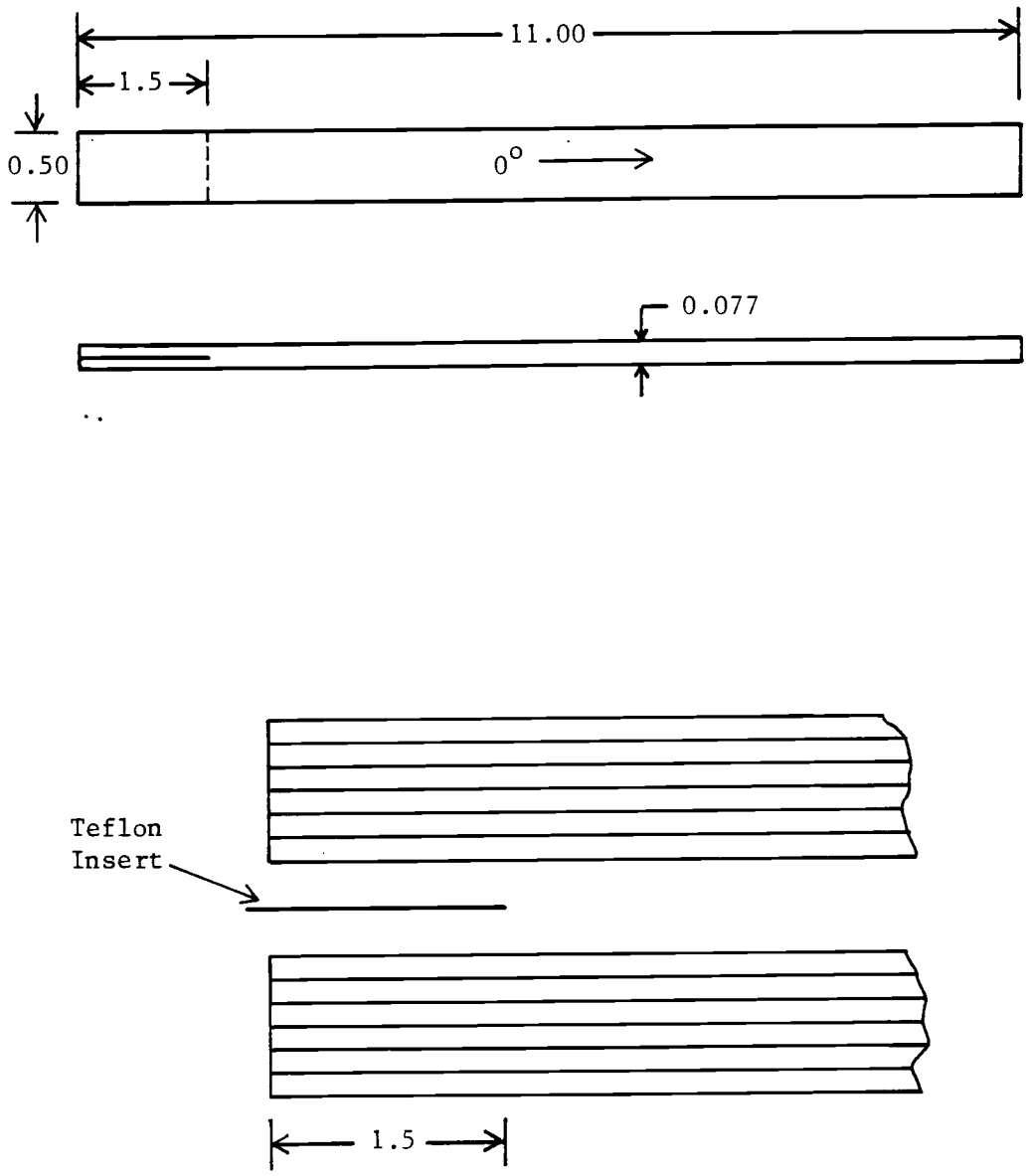

Figure 19. Specimen geometry for mode I DCB tests showing location of teflon insert. All dimensions are in inches.

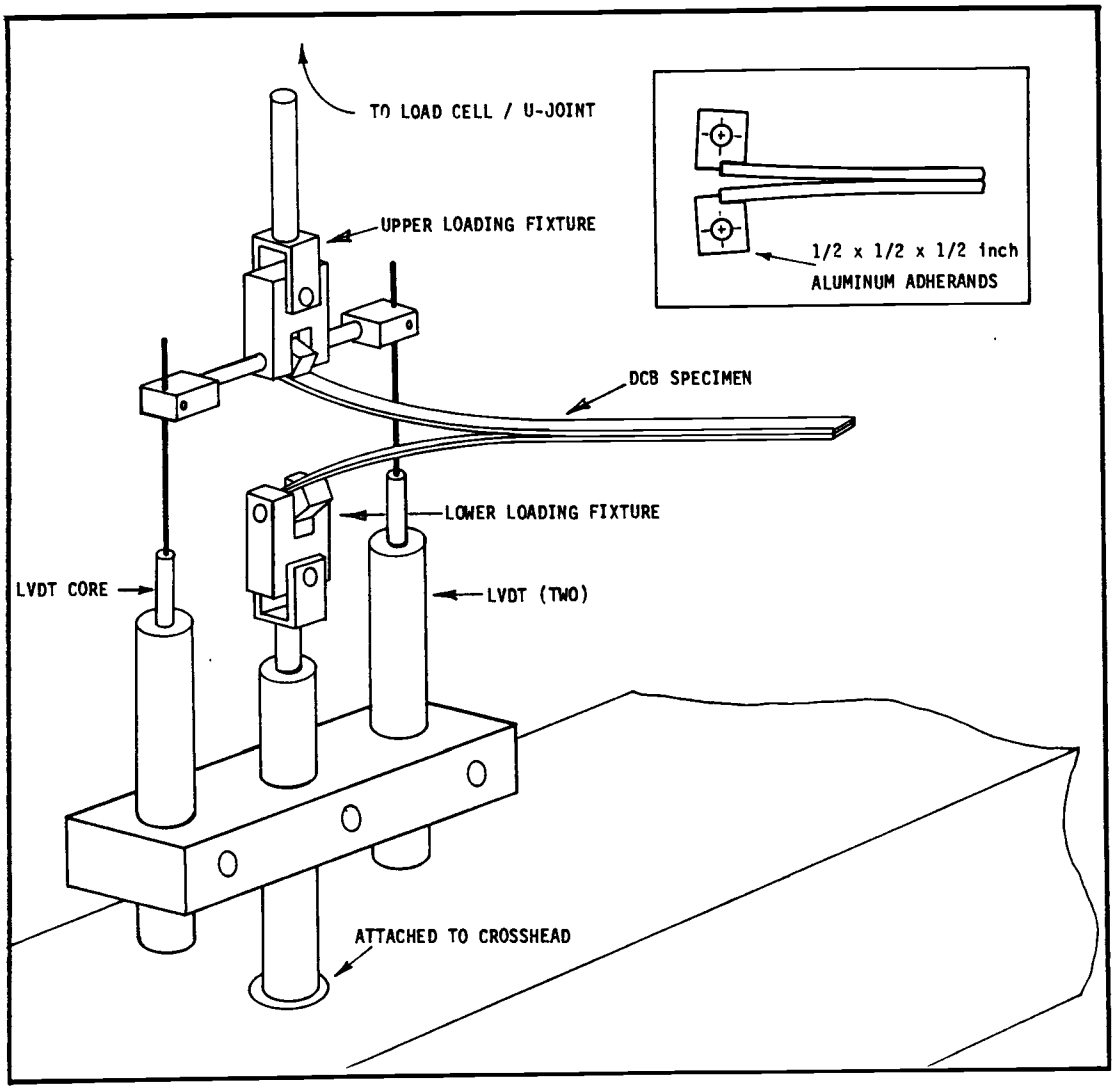

Figure 20. Mode I test apparatus. Inset shows detail of aluminum adherends and their attachment to the sample. The sample is held in the apparatus by a hinged joint. The hinged pieces are also hinged in the perpindicular direction, and both top and bottom pieces are free to rotate along the axis of loading. The LVDT's measure displacement at the loading points as the crosshead travels downward. The load is measured by a load cell which supports the upper loading fixture.

reduction at the end of each test or set of tests. After a long development period, this goal was reached. Data acquisition for all tests was computer controlled and stored on magnetic tape. All intermediate and final results were available at test completion, including graphs of each test, graphs of all calculated values (e.g. G_{Ic}, J_{Ic}, P_{max}....etc.), and print outs of results.

Specimen Testing and Data Reduction

The mode I specimen jig is diagrammed in Figure 20. The caption explains most of the features of this apparatus. The loading fixtures were pin ended so as to allow rotation in any direction. The other end of the specimen was simply supported by a loose rubber band to align the specimen prior to the test. At the start of the test the specimen is placed in the fixture and the weight of the specimen is subtracted out by re-zeroing the Instron machine. Once all this is accomplished, the test is ready to begin. It should be noted that the LVDT's are measuring the displacement at the point of loading. With the sample in place, the operator imputs the crack length on the computer and starts the machine. To eliminate any slack in the loading fixture the specimen is initially loaded to 0.5 lbs. This initial load is later accounted for by performing a linear regression on the first 10 of 100 points of the load-displacement curve and extending the straight line through zero load. As the test begins, the machine pulls the sample in tension and the computer records the load-displacement data. This continues until a crack advance is noted (operators found that audible and visual clues made crack advance apparent) at which point the machine is stopped and the crack is allowed to arrest. The crack tip

location is then marked with the aid of a magnifying glass. After the crack has arrested, the computer stops taking data and outputs a load vs. displacement curve (Figure 21). The computer then calculates compliance, area under the curve, and the linear G_{Ic}. These parameters plus the maximum load and displacement at maximum load are marked on the graph. Compliance is calculated by performing a linear regression on the P versus Δ until the P-Δ curve deviates substantially from the straight line (this is approximately the lower 1/4 of the curve). The area under the P-Δ curve is calculated using a point to point trapezoidal fit so as to allow the P-Δ curve to take any shape, linear or nonlinear. This information is stored and later used in the J integral calculation. The linear G_{Ic} value is calculated using Equation 22.

The computer then records the load-displacement data, test identification, and crack length on magnetic tape for permanent file. This entire process is performed internally by the computer thus saving a substantial amount of time for data analysis. During the output period the operator has measured the resulting crack growth and taken the test machine to zero load and is now ready to begin a new test.

Once all the tests are completed on a sample (usually 25), the computer then outputs a plot of all calculated results up to this point (Figure 22). Included on this plot are compliance, maximum load, maximum displacement and linear G_{Ic}; all versus crack length. After this, the compliance calibrated G_{Ic} is calculated using 2nd, 3rd, and 4th order polynomial fitted data and the results are plotted along with the linear G_{Ic}'s (Figure 23).

Next, the energy data used to calculate J is plotted on a graph

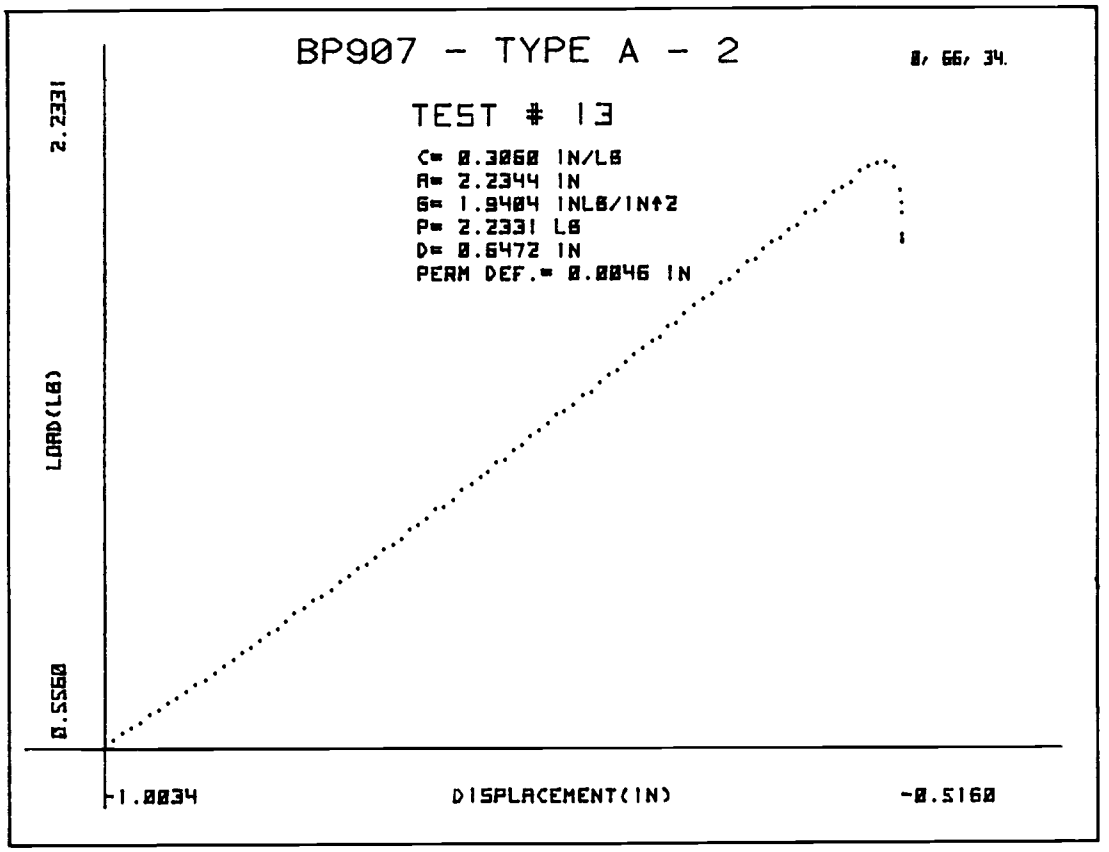

Figure 21. Typical load-displacement curve. This load-displacement is typical of that outputted at the conclusion of each crack extension. On it the computer has printed the values of compliance, crack length, linear G_{Ic}, maximum load at failure, displacement at maximum load, and permanent deflection in the DCB specimen. The numbers in the upper right hand corner refer to the tape location where the data was stored.

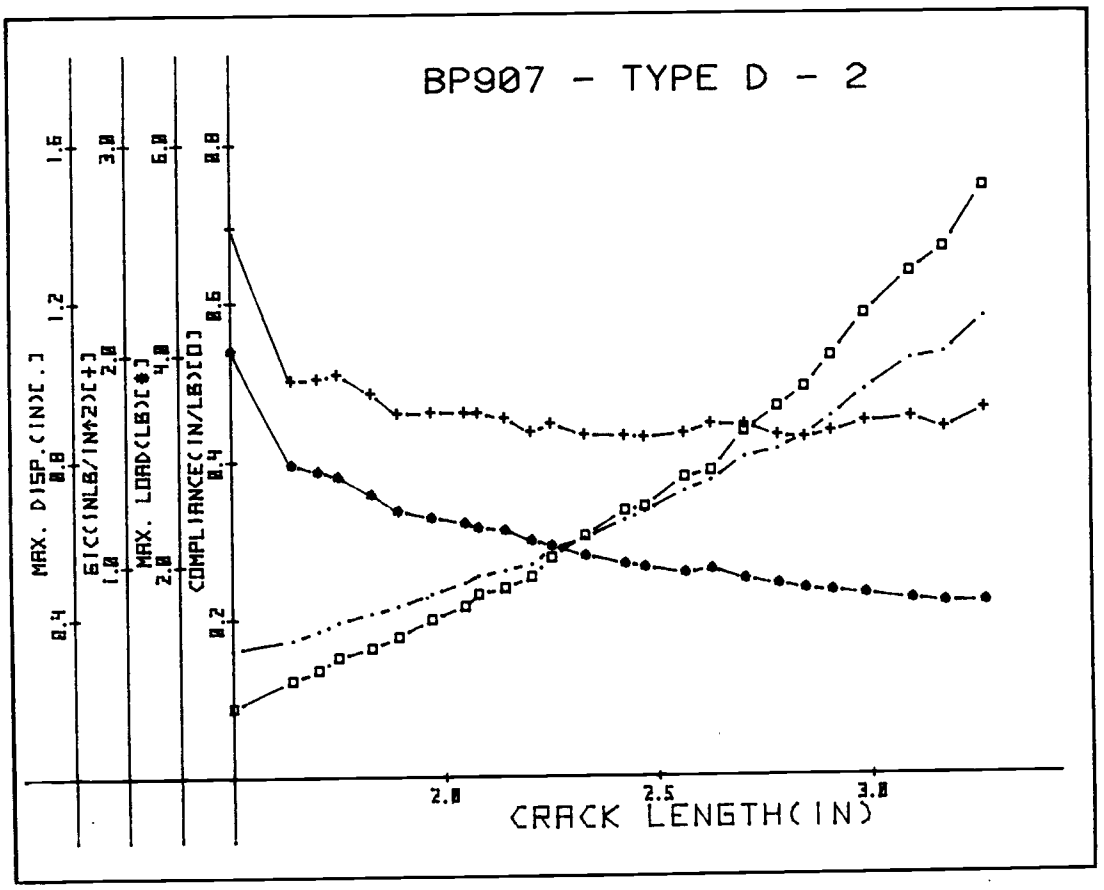

Figure 22. Cumulative plot of data from a specimen test. This type of plot is output by the computer at the conclusion of all tests on a particular sample, where compliance, maximum load, G_{Ic}, and maximum displacement are plotted as a function of crack length. The initial high value of G_{Ic} is a crack pop-in value and is not included in the average.

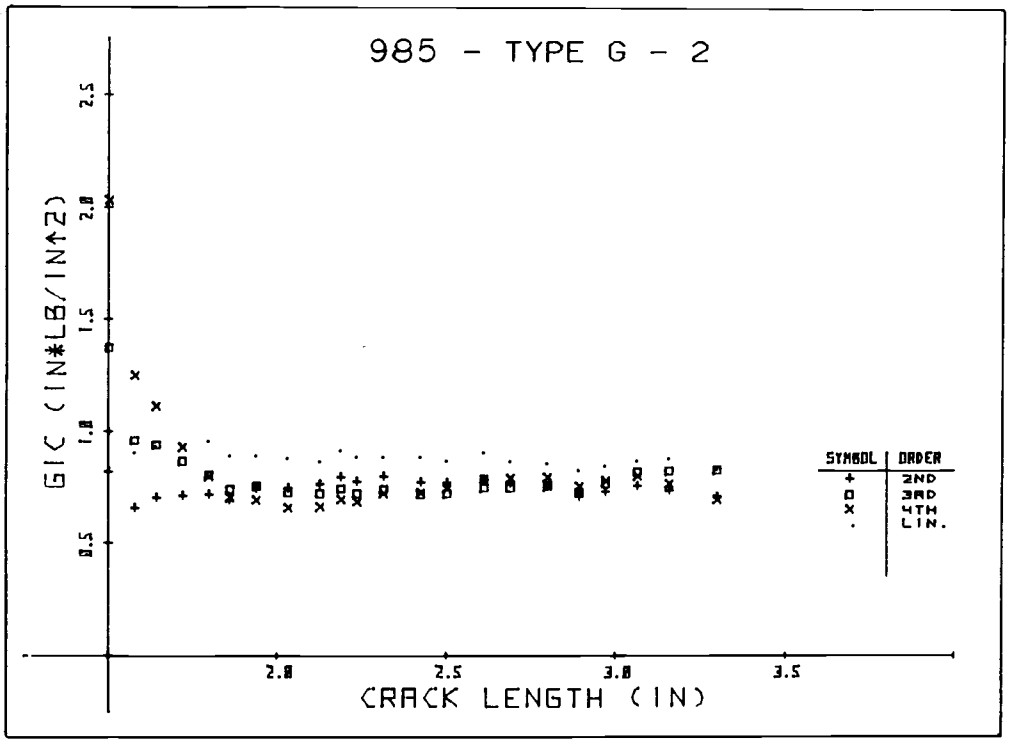

Figure 23. Plot of linear and compliance calibrated G_{IC}. This is a typical plot of compoiance calibrated G_{Ic} values obtained at the conclusion of a specimen test. Second, third, and fourth order polynomial fits of the compliance versus crack length data are used to obtain the three fitted G_{Ic} values. In addition, the linear G_{Ic} values are also shown for comparison.

using both 3rd and 2nd order polynomial fits to represent the data (Figure 24a and 24b). The energy data is constructed in two ways. First, calculations using incremental displacements of 0.03" are performed on the load-displacement data and energy versus crack length curves are developed for each displacement. This energy data is later used to give a smooth representation of the J versus crack length curves. Using this approach, however, does not enable one to determine the point of J_{Ic}, because it is unlikely than any of the equally spaced displacement increments will correspond to a maximum displacement. In order to obtain J_{Ic}, a second set of energy calculations are performed using the maximum displacements (instead of incremental displacements) from the load-deflection curves. The sole purpose of this is to extend the J_I curve to the point of J_{Ic}.

After examining a number of specimens it was determined that 3rd order fits best represent the data for smaller displacements whereas 2nd order polynomial fits best represent the data from larger displacements. By comparison of the curves in Figures 24a and 24b it may be observed that the energy data trend for small displacements suggests a flat region followed by increasing curvature. The constant curvature of a 2nd order fit is unable to represent this trend as well as a 3rd order fit. When examining the curves for larger displacements, the extra curvature from the third order fits is no longer needed. In fact, due to less data points, the third order fits are undesirable. The data for large displacements is best represented using 2nd order fits as shown in Figure 24b. However, to avoid any bias in determining when to switch from 3rd order to 2nd order fits (since this may change from specimen type to specimen type), only 3rd

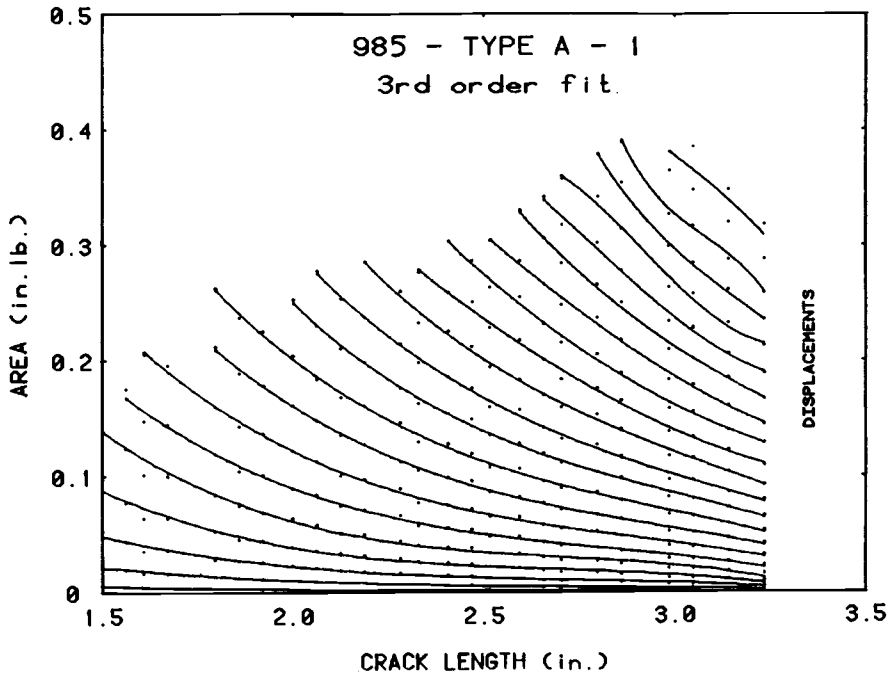

Figure 24a. Typical energy data (area vs. crack length) using 3rd order polynomial fits.

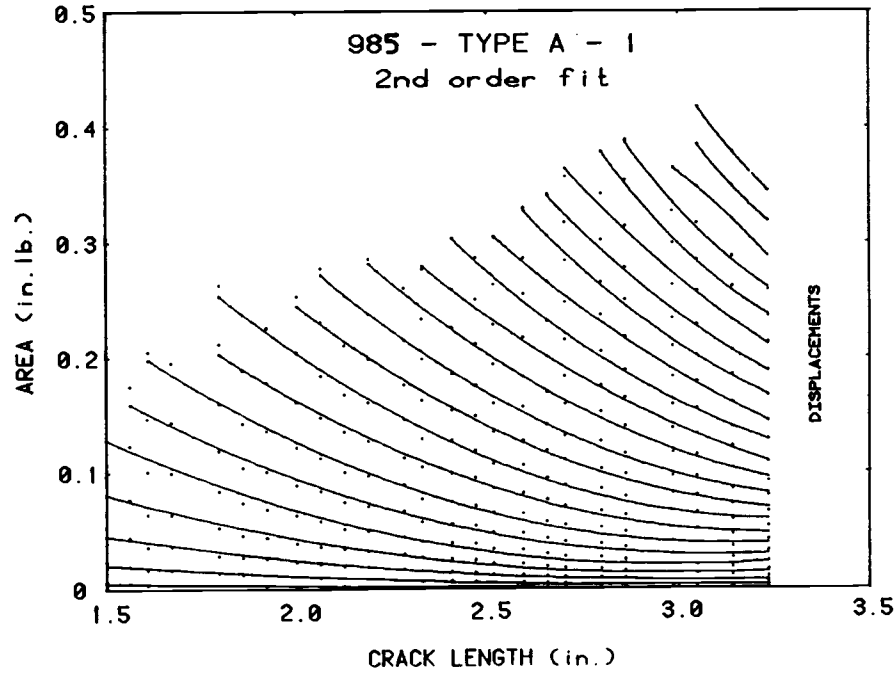

Figure 24b. Typical energy data (area vs. crack length) using 2nd order polynomial fits.

order polynomial fits are used when constructing J curves.

The J curves are constructed by using Equation 13 in conjunction with the slopes of the third order fitted energy curves, $\frac{\partial U}{\partial a}$, at constant crack lengths (Figure 24a). At smaller crack lengths the J curves are smooth and the data is believed to be well represented. At larger crack lengths, however, the data used to construct the J curves is poorly represented by the large displacement 3rd order fitted energy curves (See Figure 24a) as discussed above. Subsequently, these curves were disregarded.

The point at which J_{Ic} occurs may be determined from the maximum displacement of each particular crack length. As discussed above, the energy curves are constructed on both an equal displacement basis and a maximum displacement basis. The equal displacement energy curves are used to develop J curves up to a point close to maximum displacement for a given crack length. The maximum displacement energy curves are then used to extend the J curves to the point of J_{Ic}.

Although these J curves are plotted versus displacement, a similar procedure may be used to plot J curves versus load. In either case the J curves give a well defined representation of how a particular material will react for a given crack length. They provide a meaningful way of comparing data from different types of material.

Results and Discussion

Under a contract funded by the Boeing Company, over 90 specimens were tested for mode I interlaminar fracture toughness. These consisted of three baseline resin systems with various filler modifications added to each resin system. The purpose of this study was not to compare the effects of the various modifications made to the baseline materials, but rather to present a consistent reliable method of developing mode I fracture toughness parameters for composite materials.

Results of all tests showing the average critical failure energies obtained by the various approaches are shown in Figure 25. Each average value is representative of data obtained from the three specimens of the particular material type. All averages exclude the pop-in value (the value from the first crack jump). The calculations of averages for the linear and compliance calibrated approaches were straightforward (e.g. the average of all data points). Since original calculations dealt only with critical failure energies, the average values of J_{Ic} were determined directly from the fitted energy curves (e.g. the tips of the maximum displacement energy curves).

Examination of the data in Figure 25 indicates that the linear elastic interpretation of critical failure energy normally gives the highest values whereas the compliance calibrated and J integral approaches generally yield slightly lower results. If one considers the nonlinearity in the load-deflection curves (Figure 21), then the J integral approach would be assumed to be the method that would best represent the data. With this in mind, the linear elastic and compliance calibrated approaches result in an overestimate of actual

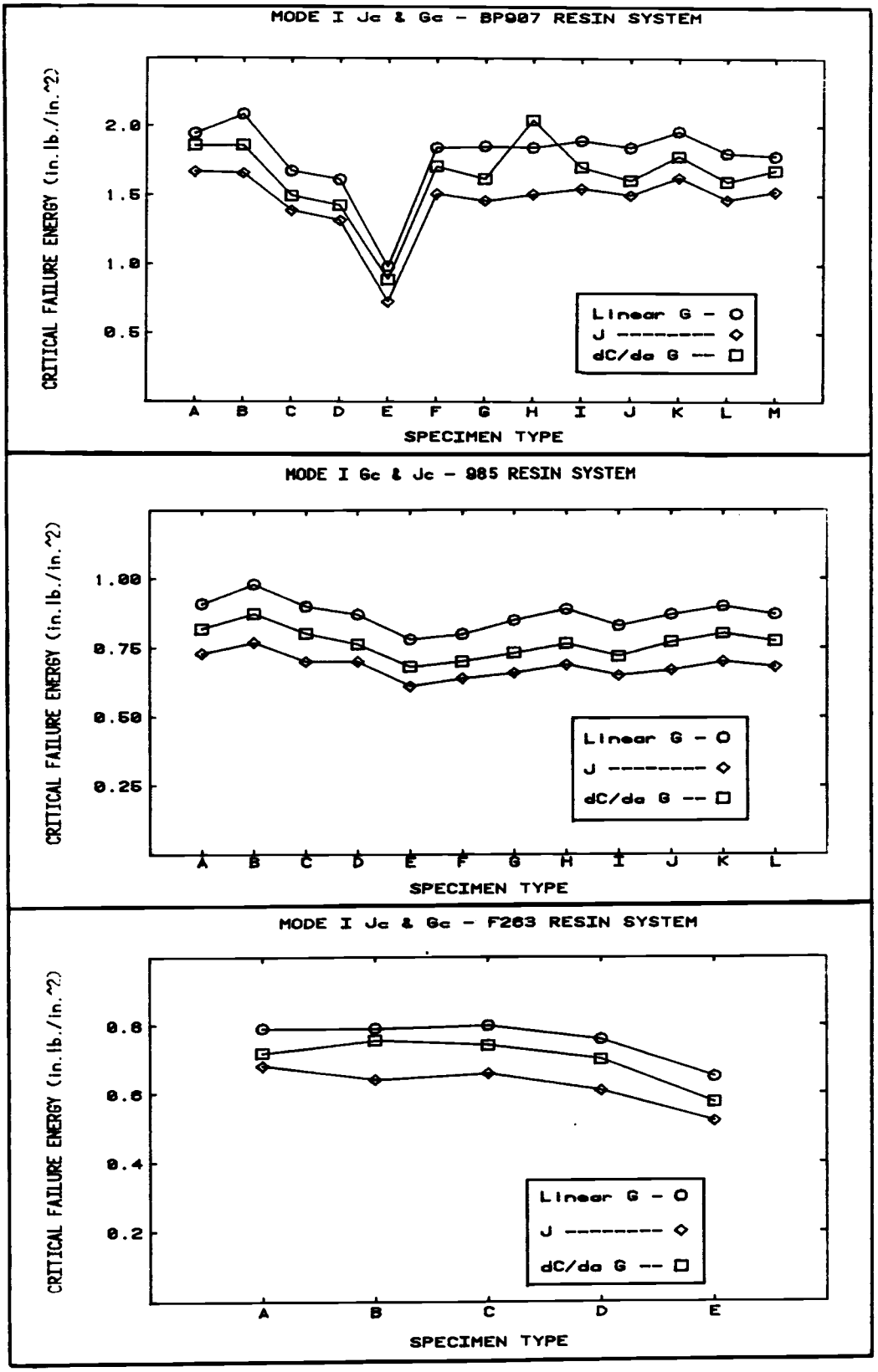

Figure 25. Mode I critical failure energies.

critical failure energy. For materials that exhibit higher degrees of nonlinear behavior, this overestimate (or underestimate if the case may be) of critical failure energy may be substantially higher than what was observed with the specimens in this program.

When determining which analysis method would best characterize critical failure energy, a number of experimental observations were made. Upon experimentally checking the assumption of a constant bending modulus made in deriving the linear equation, it was observed that the bending modulus monotonically increased with beam length. This phenomena was observed in mode I tests as well as bending tests performed on uncracked specimens with various beam lengths (Figure 26). At crack lengths ranging from 1.5" to 3.5" this increase in bending modulus was observed to be as much as 25%. Similar results were observed by Vanderkley[44] in which mode I and mixed mode tests were performed on composite DCB specimens (0.1 inches thick) with crack lengths ranging from 4.0" to 5.7". Vanderkley found that the apparent bending modulus increased at short crack lengths but tended toward a constant value at longer crack lengths. It appears that the composite specimens tested in this program respond in a manner that is contrary to small deflection, linear beam bending theory.

Figure 27 graphically represents the effect of assuming a constant bending modulus. shown in this figure are four load displacement curves of the same specimen obtained from four crack lengths. The dotted lines represent the actual load-displacement curves which were obtained in the experiment. The solid lines show the curves which were obtained from the linear beam bending equation using a constant modulus derived using experimental data from the first test (at a=1.5). From

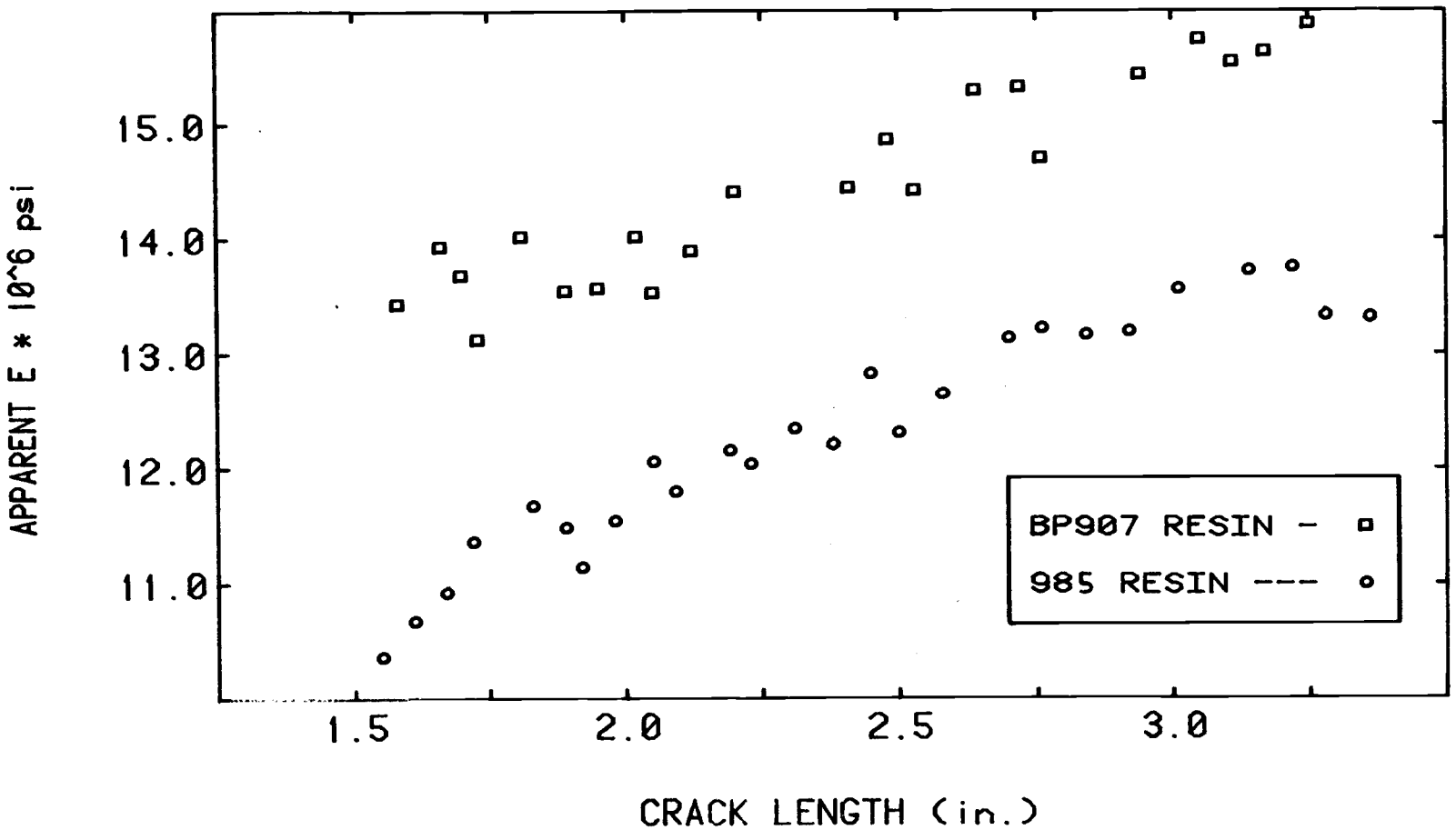

Figure 26. Apparent flexural modulus as a function of crack length using small deflection, linear beam bending theory.

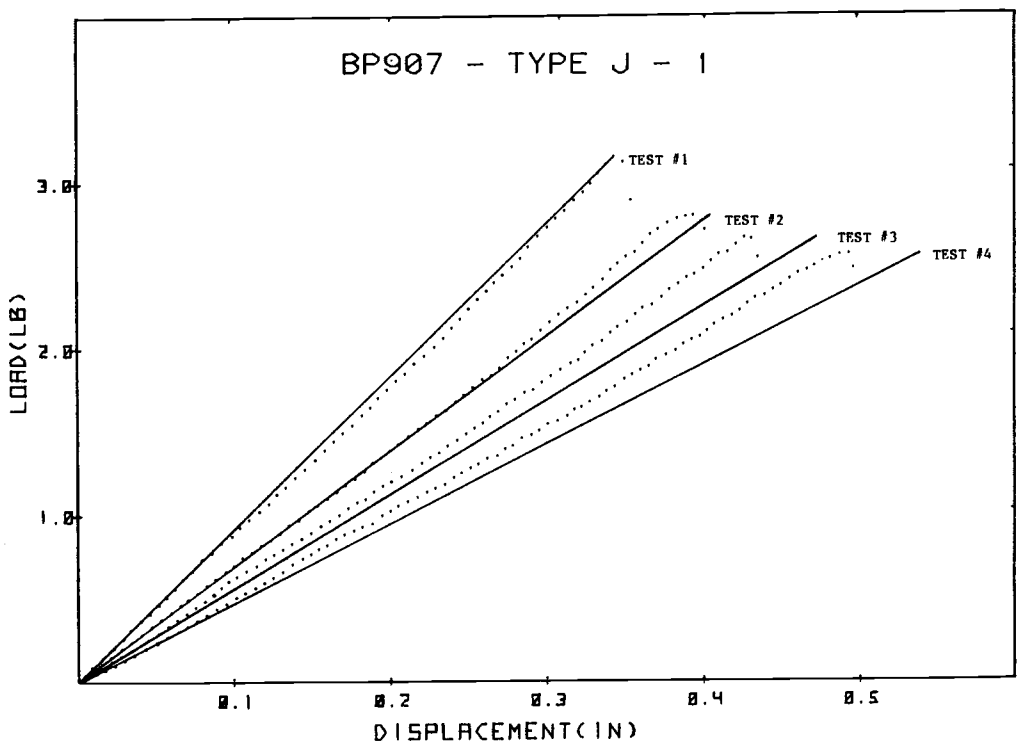

Figure 27. Graphical representation of assuming a constant bending modulus. The dotted lines represent experimentally obtained load-displacement curves. The solid lines show the curves obtained from the linear beam bending equation using a constant bending modulus.

this, one may interpret the overestimate of using the linear G_{Ic} approach (Equation 20) when a constant modulus is assumed. The real effect of the monotonically increasing E is not as drastic in actual calculations as it appears in Figure 27. The reason for this is that the equation used for G_{Ic} in the current investigation utilizes crack length, load and displacement to calculate G_{Ic} (e.g., E has been substituted out of the equation). This procedure is equivalent to allowing E to vary with crack length as it does when back calculations using the linear equation are performed.

The compliance calibrated method of determining G_{Ic} is also found to be a slight overestimate. This is assumed to be due to the nonlinear nature of the material tested. Compliance calibrated G_{Ic} assumes linear elastic material behavior whereas the material which was tested exhibited some nonlinear elastic behavior. As a result, when applying the compliance calibration approach, the maximum displacement corresponding to maximum load is greater than actual experiments show (Figure 14). A more conservative approach would be to use the compliance calibrated load in Equation 17 that corresponds to the experimentally calculated maximum displacement rather using the actual maximum load.

An extensive amount of work has been performed to characterize cantilever deflection of thin flexible beams, similar to those examined in this study [2, 3, 5, 8, 21, 22, 25, 29]. This has been applied to both linear and nonlinear materials. As previously discussed Devitt[11] studied the large deflection problem using a method proposed by Bisshopp and Drucker[5]. This dealt primarily with large deflecticns of specimens exhibiting linear material behavior. The

problem of large deflection of cantilever beams of nonlinear materials has been studied by Prathap and Varadan[29] and Lewis and Monasa[21]. Their results show interestingly that at low values of (Pa^2/EI), beam tip deflections are larger than those predicted by small deflection theory for linear materials. Figure 28 shows beam tip deflections for a uniform cantilever beam using linear material, small deflection theory (e.g. simple beam theory), linear material, large deflection theory (e.g. Bisshopp & Drucker)[5], and nonlinear material, large deflection theory (e.g. Prathap & Varadan). This figure is similar to that shown by Prathap and Varadan[29]. Note the variation in beam tip deflection between the three curves at values of Pa^2/EI less than 1.3. At values of Pa^2/EI approximately equal to 1.3, the beam tip deflections obtained assuming linear material behavior with small deflection theory tend to equal those obtained assuming nonlinear material behavior with large deflection theory (Figure 28). If one were to assume linear material behavior when testing a nonlinear material, an apparent increasing flexural modulus would be observed. All of the specimens examined in this study were tested at lower ranges of Pa^2/EI (i.e. approximately 0.2 to 0.8), which is precisely the range in which apparent increasing flexural modulus values (due to assuming a linear material but actually testing a nonlinear material) would appear.

This apparent increasing flexural modulus in composite materials has also been investigated by other authors. Zweben et. al.[45] investigated the effect of small span-to-depth ratios on the flexural modulus of three-point bending composite specimens. Their results, indicated that the apparent flexural modulus increases as span-to-depth

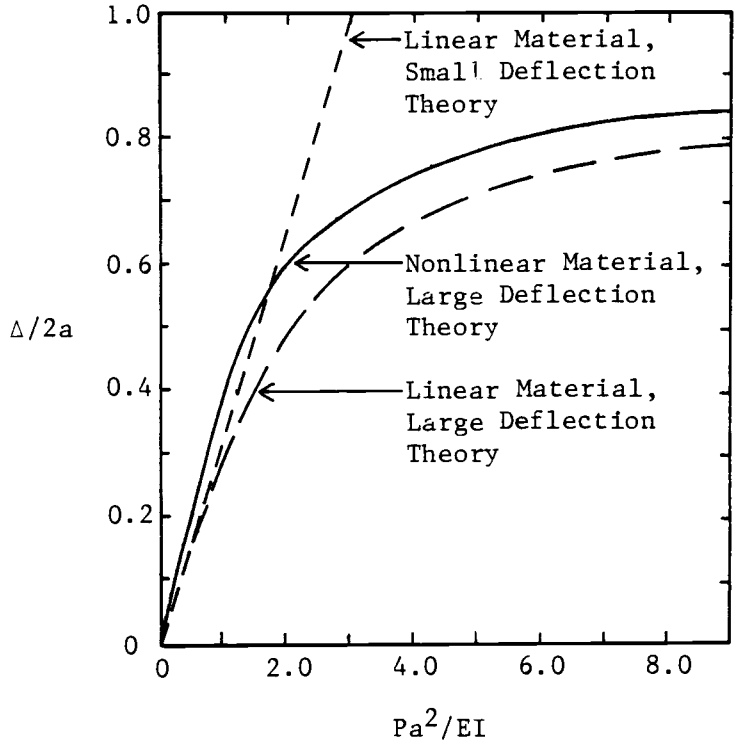

Figure 28. Tip deflections for a uniform cantilever beam as described by Prathap and Varadan (29).

ratio increases. They believed the reason for this increase was due to a contribution of shear deflection which would add to the small deflection linear beam tip equation (Equation 18). Normally, for isotropic materials this contribution of shear deflection is very small and may be neglected. However, for composite materials the ratio of extensional modulus to shear modulus is very large (approximately equal to 90). Omitting the contribution from shear deflection may account for an increasing flexural modulus. It is quite possible that the increase in flexural modulus observed in this program may be due to a combination of nonlinear material behavior and low shear modulus values.

It is important to realize that composite materials similar to those tested in this program are not isotropic materials and their behavior may not always follow that of linear isotropic theory. Because composites are composed of two very distinct phases, interactions between fibers and matrix may result in behaviors much different from behaviors normally exhibited by conventional isotropic materials. Internal characteristic properties of composites such as those of the fibers and matrix should be considered. Characteristic dimensions and microstructure appearance (e.g. presence of voids, fiber content and orientation, resin starved and resin rich areas...etc.) are important features which should be addressed when analyzing these materials.

This brings up a question regarding the validity of using the linear G_{Ic} approach as a method for determining critical failure energies for composites and other materials that exhibit nonlinear behavior. Using linear small deflection theory to simplify expressions

for critical failure energy implies that the material is linear and has a constant bending modulus, regardless of beam length. This was found to be untrue for the specimens tested in this study and may be a major reason for the discrepancies obtained when using the J_{Ic} approach versus the linear G_{Ic} approach.

Another phenomena which was observed during the testing process was the fact that a permanent deflection was found to exist between the two beam halves of the DCB specimen at the end of a set of tests. When the specimen was brought back down to zero load, the two beam halves did not close together. This permanent deflection was found to increase as subsequent tests were performed on the same specimen. A typical plot of the permanent deflection as a function of crack length is shown in Figure 29. Although it appears to be very small, this permanent deflection must be subtracted out of the calculations or an overestimate of critical failure energy may occur. For example, the J integral approach assumes that each load-deflection curve begins at zero load and zero deflection (all P-Δ curves have the same origin). After each test, a small amount of permanent deflection is added to the specimen. If not accounted for, this will change the origin of the load-deflection curves as opposed to that of the initial test, thus changing the shapes of the energy versus displacement curves.

Consider the load deflection curve shown in Figure 30. These experimental results were obtained by loading a cracked specimen and allowing the crack to extend over a length of approximately 0.5 inches and then unloading the specimen to zero load. The specimen was then reloaded and the same procedure was repeated. Note that when the specimen is returned to zero load a permanent deflection exists. To

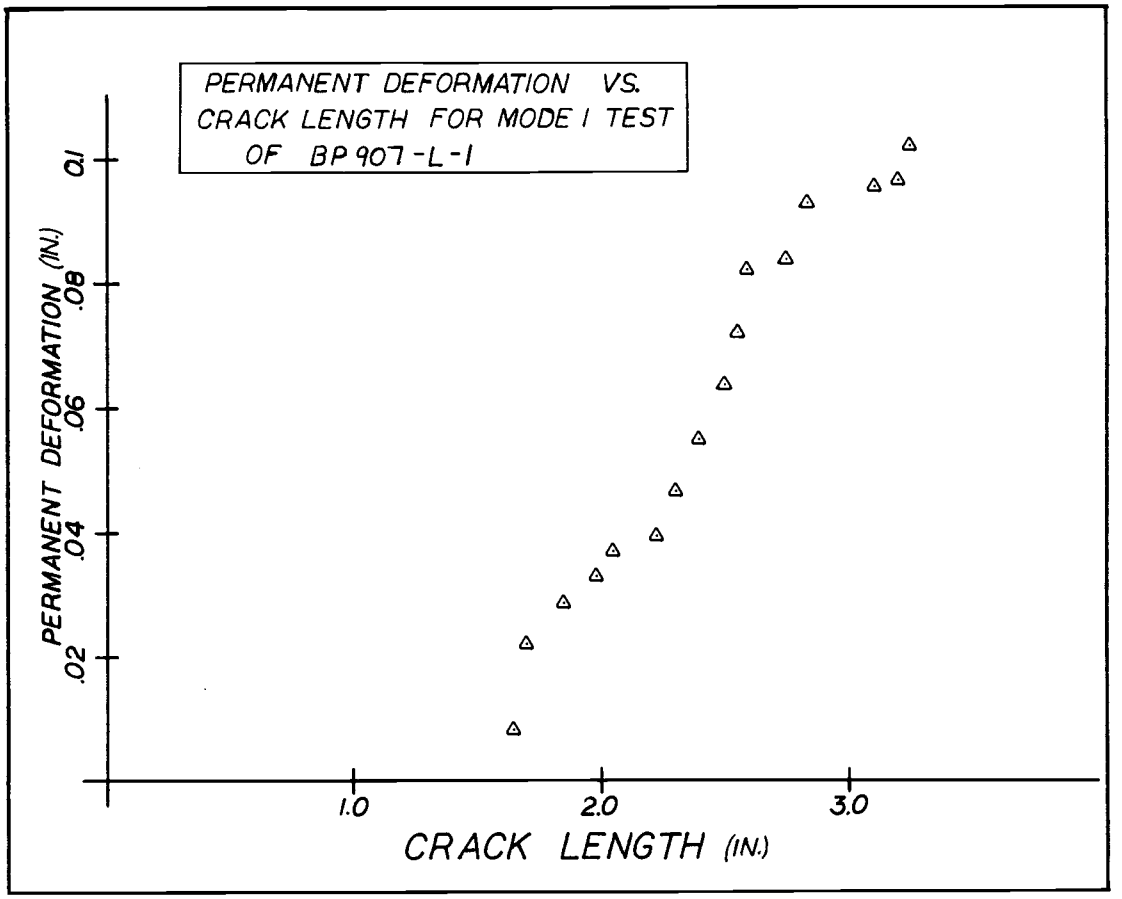

Figure 29. Typical plot of permanent deformation vs. crack length. This plot shows the permanent deformation that remains in the beam halfs of the DCB specimen as the crack increases. The permanent deformation is a result of the energy that has been expanded in plastic deformation of the beam halfs.

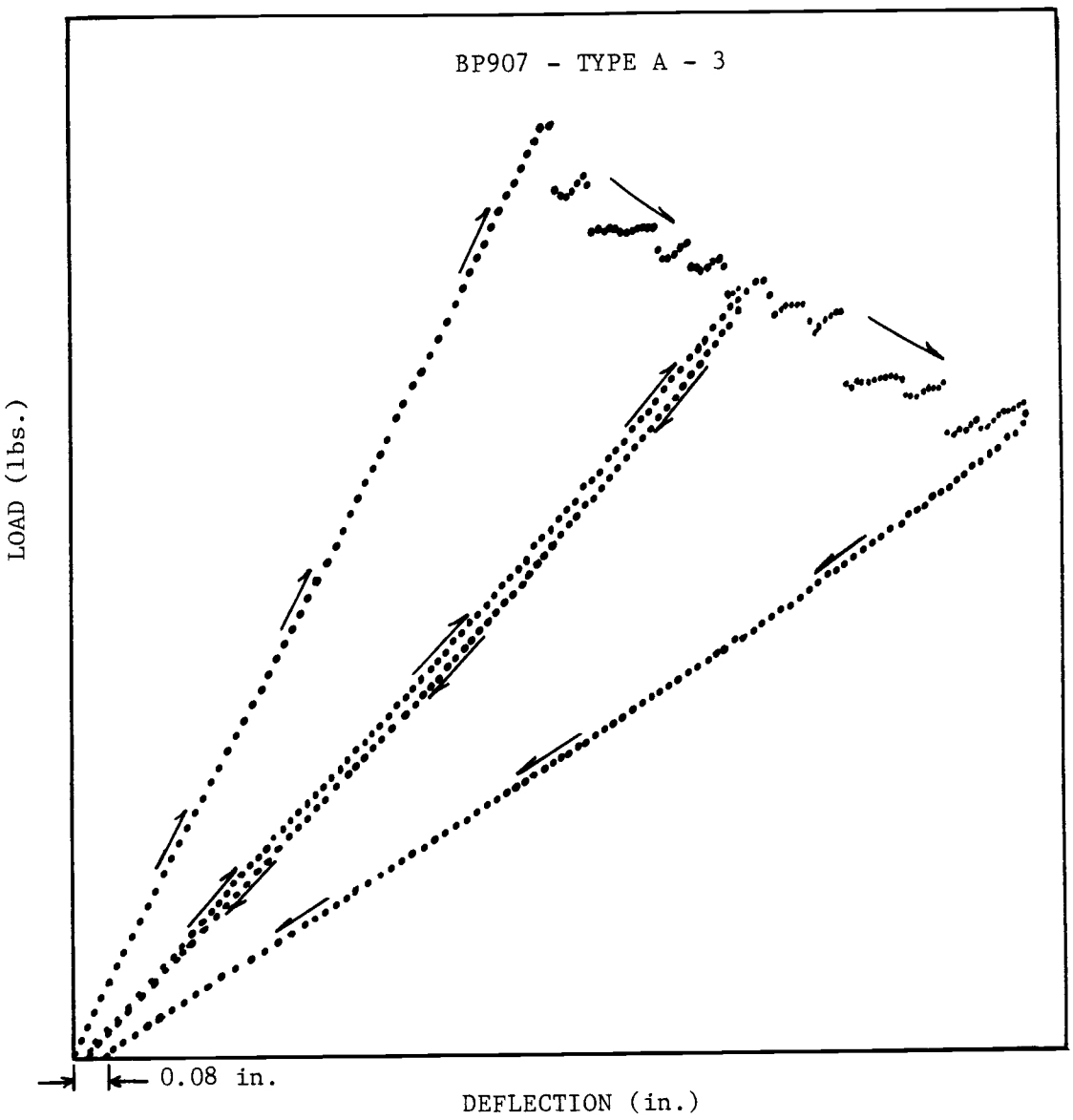

Figure 30. Load-unload curves showing permanent deflection. For each of the two load-unload curves the crack was allowed to extend over a length of 0.5 inches.

account for the permanent deflection, the origins of all curves should be positioned so as to be the same as the origin of the original curve. This requires that all load deflection curves of longer crack lengths be shifted slightly to the left.

This occurrence of a permanent deflection (or a plastic deformation) brings up some questions regarding the nature of double cantilever beam testing in which repetitive tests are performed using the same specimen. Materials which behave linear elastically to failure are ideally suited for DCB testing because no plastic or permanent deflection occurs within the specimen (except at the very crack tip) and the same specimen may be used to collect a large amount of data. However, for materials that exhibit large amounts of plasticity, repeated tests on a DCB specimen may or may not give a true representation of that material's critical failure energy. For highly elastic-plastic materials the occurrence of plasticity changes the material's inner structure. This may result in load deflection curves being different for materials that have never been stressed versus identical materials that have undergone past loading histories. Landes and Begley[20] state

> "It has not been shown that loading a cracked body and then extending the crack under load will give the same result as initially extending the crack and then loading."

The materials in this study did exhibit some degree of nonlinearity. To determine if this was nonlinear elastic or elastic-plastic behavior a specimen was loaded to various levels without causing any crack extension. It appears from Figure 31, that the material exhibits nonlinear elastic behavior as opposed to elastic-

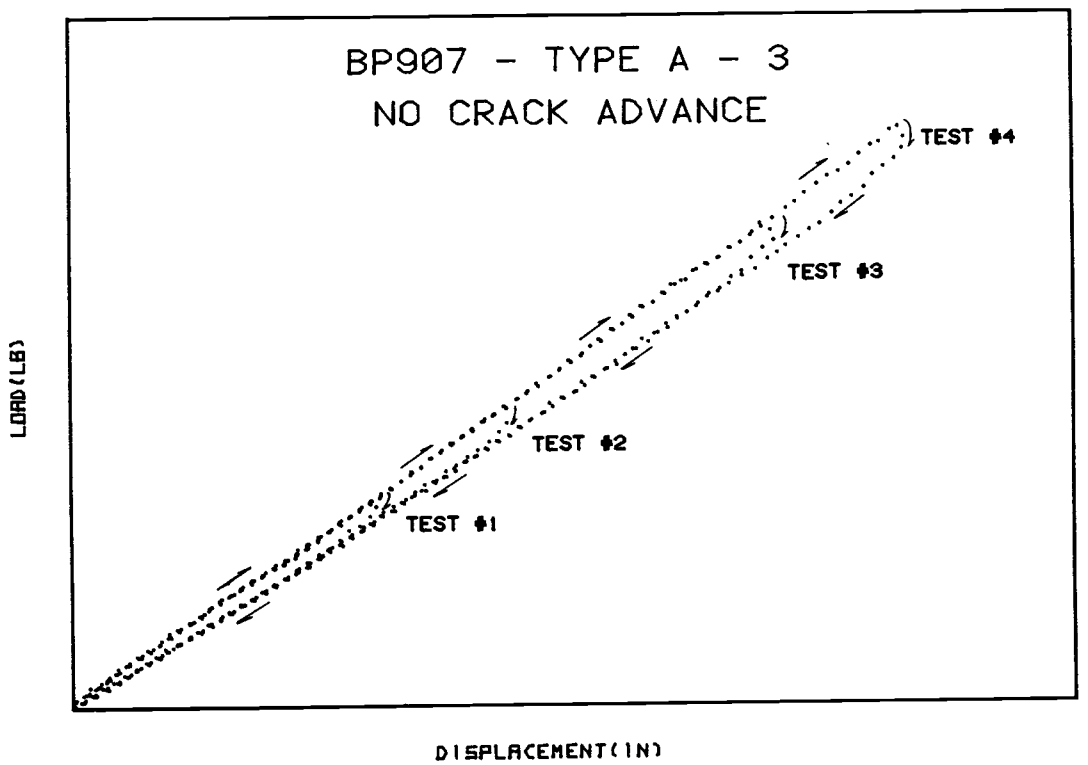

Figure 31. Load-unload curves of BP907 - TYPE A - 3 specimen with no crack advance. This specimen was loaded then unloaded to four different stress levels without any crack advance. The slight upward nonlinearity indicates a nonlinear elastic material behavior.

plastic behavior. The permanent deflection which was observed occurs only after crack extension. This permanent deflection is believed to be a result of matrix cracking or slip between fibers and matrix which occur during crack extension. These matrix deformations continually build up along the arms of the DCB specimen as the crack length gets longer. Microscopic examinations of the specimens revealed this was indeed the case.

In regards to the J integral approach, it was previously mentioned that original J_{Ic} values were determined by taking the maximum slope of the energy curves directly. Eventually, plotted values of J versus displacement showing the behavior of the material up to and including the point of failure were included in the analysis. J_{Ic} was determined from these J curves where the point of maximum displacement occurred.

The advantage of the J curves is that the value of J_{Ic} does not rely on one point only (e.g. the maximum slope of the energy curves). Instead, all the data is utilized giving a clear representation of what is happening within a material up to the point of crack extension.

Consider the J curves shown in Figure 32. These were obtained from the baseline (Type A) American Cyanamid BP 907 specimens. The J curves are constructed on a point to point basis. For each curve, as the J value nears the critical J_{Ic} region the slope of the curve becomes somewhat irregular. This type of behavior was typical of all specimens examined. It has also been observed in fracture toughness tests performed on particleboard in which the J integral analysis was used[15].

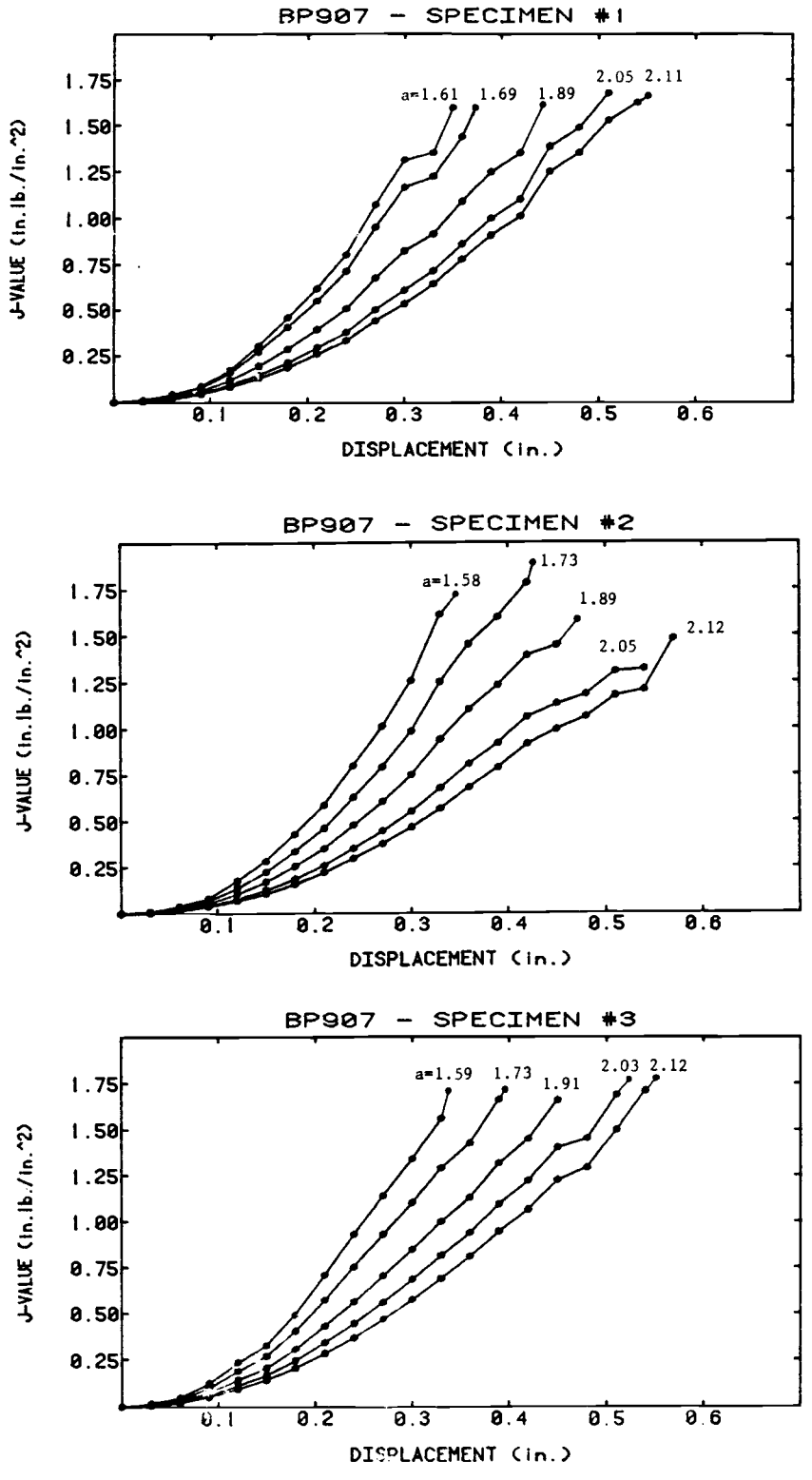

Figure 32. J versus displacement curves for three BP907 - TYPE A specimens. The numbers at the top of each curve refer to respective crack lengths.

There are a number of reasons which may account for this. One is that matrix cracking and fiber breakage may be occurring near the crack tip as the load approaches the point of crack extension. If this was the case, the upper regions of the load deflection curves should straighten out or bend off instead of exhibiting the slight upward nonlinear behavior seen in the lower and middle portions of the curves (Figure 21). It was observed that the load deflection curves do bend off as crack extension approaches.

Another reason which may account for the irregular behavior at the ends of the J curves arises when using the fitted data from the energy curves. The energy curves are used to determine the partial derivative for J_I (Equation 13). The lower portions of the J curves are constructed using the lower displacement energy curves, which utilize a large number of data points to fit the experimental data. Energy data from higher displacements (which is used to construct the upper portions of the J curves) utilize fewer data points to fit the experimental data. Subsequently, the higher displacement energy curves may not give as accurate a representation of energy as compared to lower displacement energy curves.

A criteria for determining J_{Ic} may be established from the J curves. As an example, J_{Ic} may be interpreted to be the point where the J curve deviates substantially from its original shape. An average value may be obtained using J curves for various crack lengths. This would be comparable to adding a safety factor to design.

To further smooth out the J curves, energy data from sets of three identical specimens were merged, and J curves were plotted.

This was performed through a separate programming routine which utilized the experimental data which was stored on magnetic tapes. Merging information from identical specimens resulted in more data and hence better curve fits. Typical results of merging the data are shown in Figure 33. Note the smoothness of the curves from Figure 33 as compared to curves obtained from separate specimens in Figure 32. Those in Figure 33 are well behaved and yield more of an average representation of the particular material being examined.

In order to determine where discrepancies arise between the J integral approach and the compliance calibrated method, G curves were constructed using experimentally determined compliance data with the compliance calibrated equation. The compliance calibrated equation may be restated as:

$$G_{Ic} = \frac{P_{max}}{2B}\frac{dc}{da} \qquad (23a)$$

$$G_{Ic} = \frac{P}{2B}\frac{dc}{da} \qquad (23b)$$

For a given crack length, compliance ($c = \Delta/p$) and $\frac{dc}{da}$ were determined using the fitted compliance curves (See Figure 14). Since compliance is constant at a given crack length values of load (P) may be determined ($P = \Delta/c$) for given values of displacement (Δ). These were then used in Equation 23b to obtain values of G_I at various displacements.

Compliance calibrated G versus displacement curves were plotted along with J versus displacement curves for various crack lengths as shown in Figure 34. It is interesting to note that for given crack

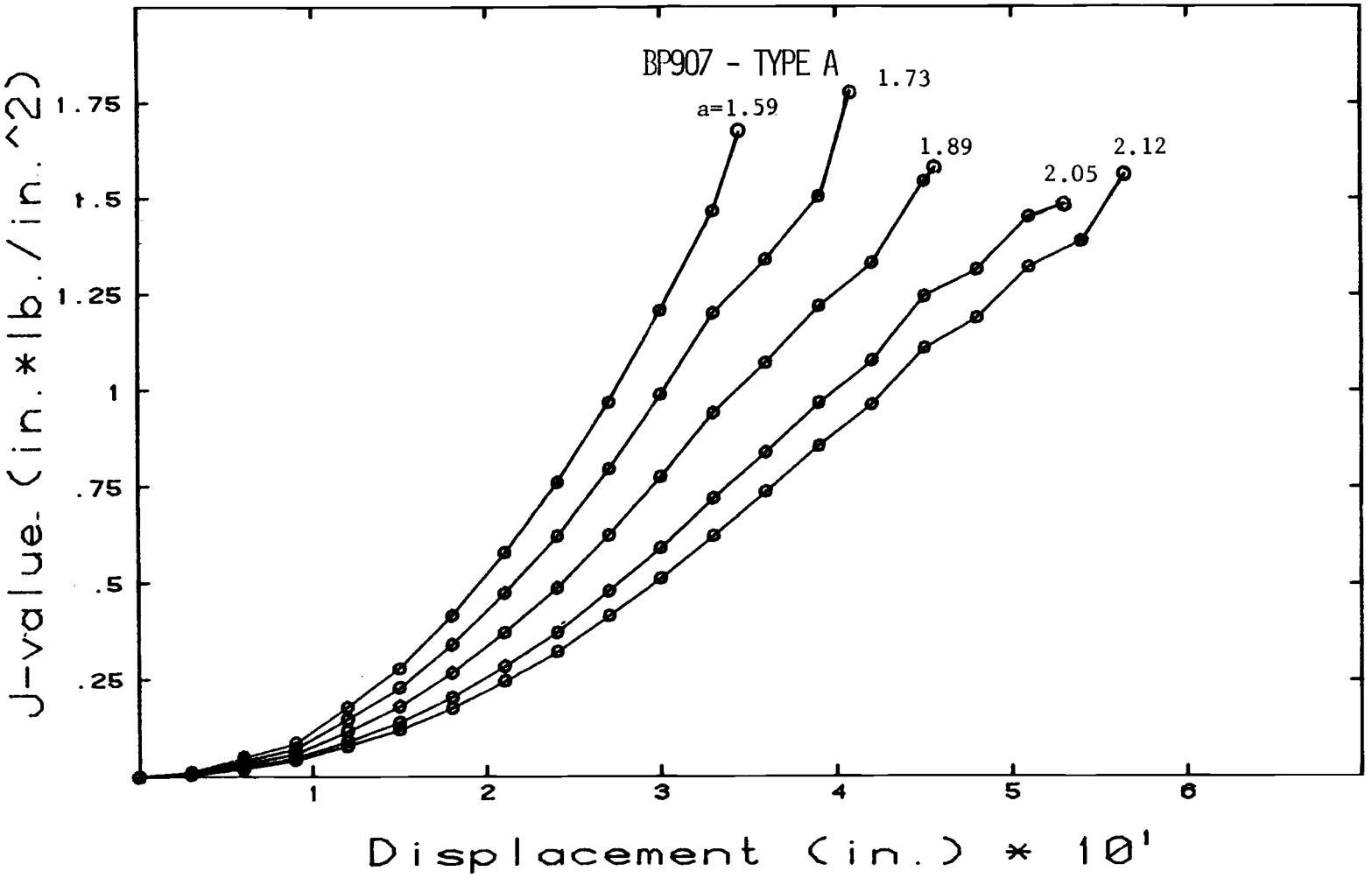

Figure 33. Merged J versus displacement curves for BP907 TYPE A specimens. These curves were obtained by merging the energy data from the three individual specimens. The numbers at the top of each curve refer to respective crack lengths.

lengths both the compliance calibrated G and the J show similar behaviors at lower portions of the curves. At upper portions of the curves, however, significant deviations begin to appear. This may be due to the fact that the actual nonlinear response becomes more pronounced as compared to the assumed compliance calibrated response at upper portions of the load-displacement curves. This is illustrated in Figure 35. The crack lengths for the load-displacement curves in Figure 35 correspond to the G and J curves in Figure 34. By comparison of the two figures it appears that deviations between the G and J curves takes place at approximately the same point where the experimentally determined nonlinear and the assumed compliance calibrated linear load-displacement responses begin to deviate.

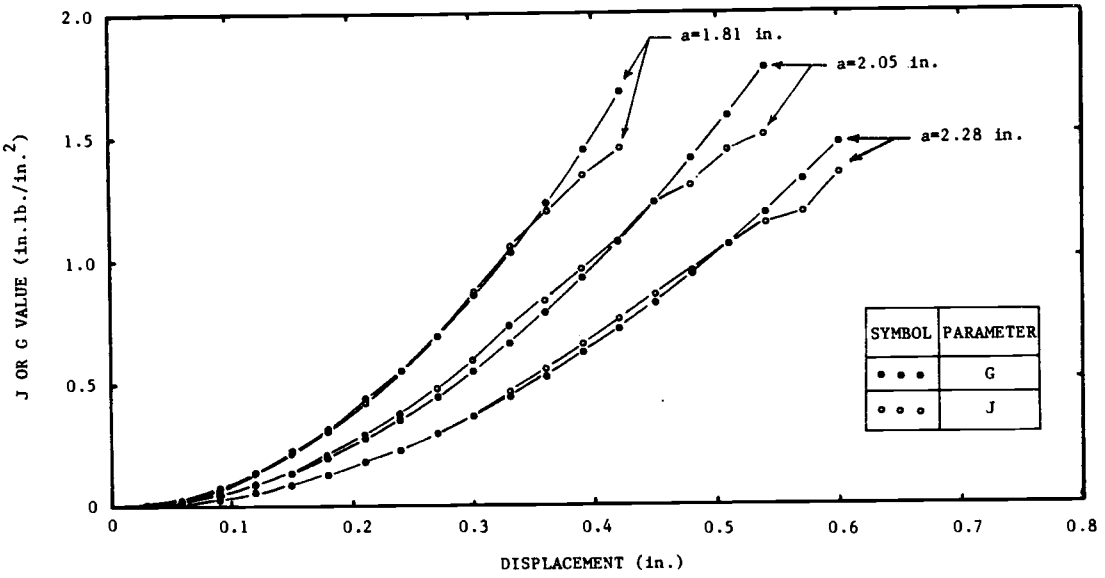

Figure 34. J and compliance calibrated G versus displacement curves for BP907 TYPE A specimens.

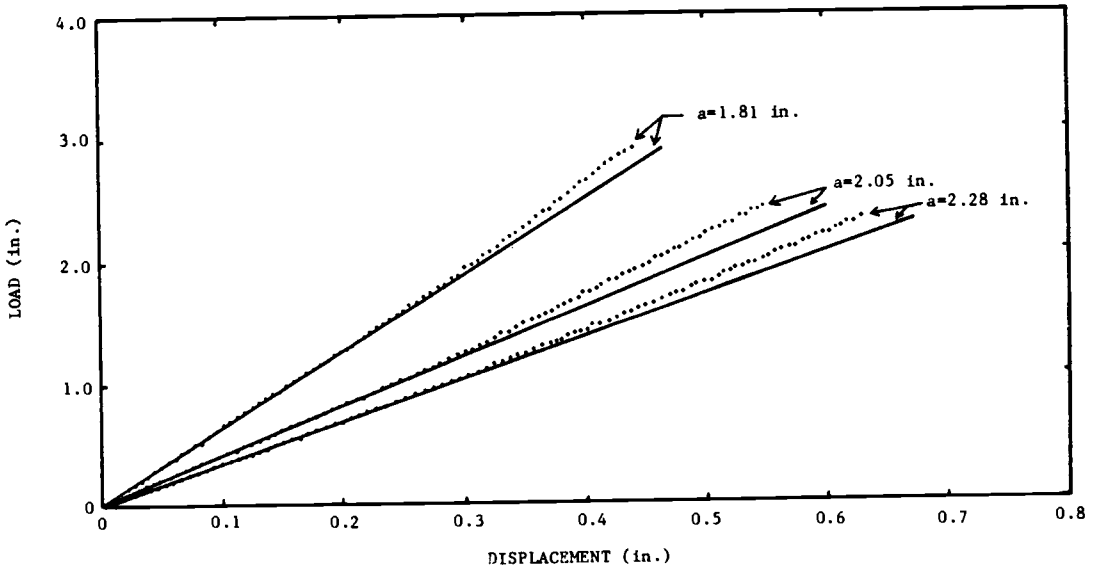

Figure 35. Experimental and compliance calibrated load versus displacement curves. The solid lines indicate the compliance calibrated curves. The dotted curves refer to experimentally obtained results.

Microscopy Studies

One of the important areas of work in regards to fiber reinforced composites is that of fractography. Much work has been done in advancing material scientists through the understanding of failure surface morphologies. With this in mind, an attempt was made to correlate fractographic observations with experimental test data. It was hoped that material surface studies would yield insight as to how or why the composite specimens reacted to delamination failure. In this section, remarks will be made regarding mode I surface appearances, crack-front interactions with the microstructure, and general observations of the interlaminar layer.

Surface Appearances

In general, the mode I fracture surface is typically flat and smooth as seen in Figures 36 and 37. Occasionally, long fibers or fiber bundles that have been separated from the resin as a result of tie zones across the crack are evident (Figure 38 and 39). Fiber pullout results in holes which are often observed (Figure 40). Very close examination reveals that extremely fine cracks exist along the resin-fiber interface, and that resin crazing is common (Figures 37, 38, 39 and 40).

All the resin systems examined presented a similar surface appearance. The BP 907 system was supposed to have a dispersed elastomeric modifier for the purpose of toughening the resin. Their presence was confirmed (Figure 37) although their distribution was not known.

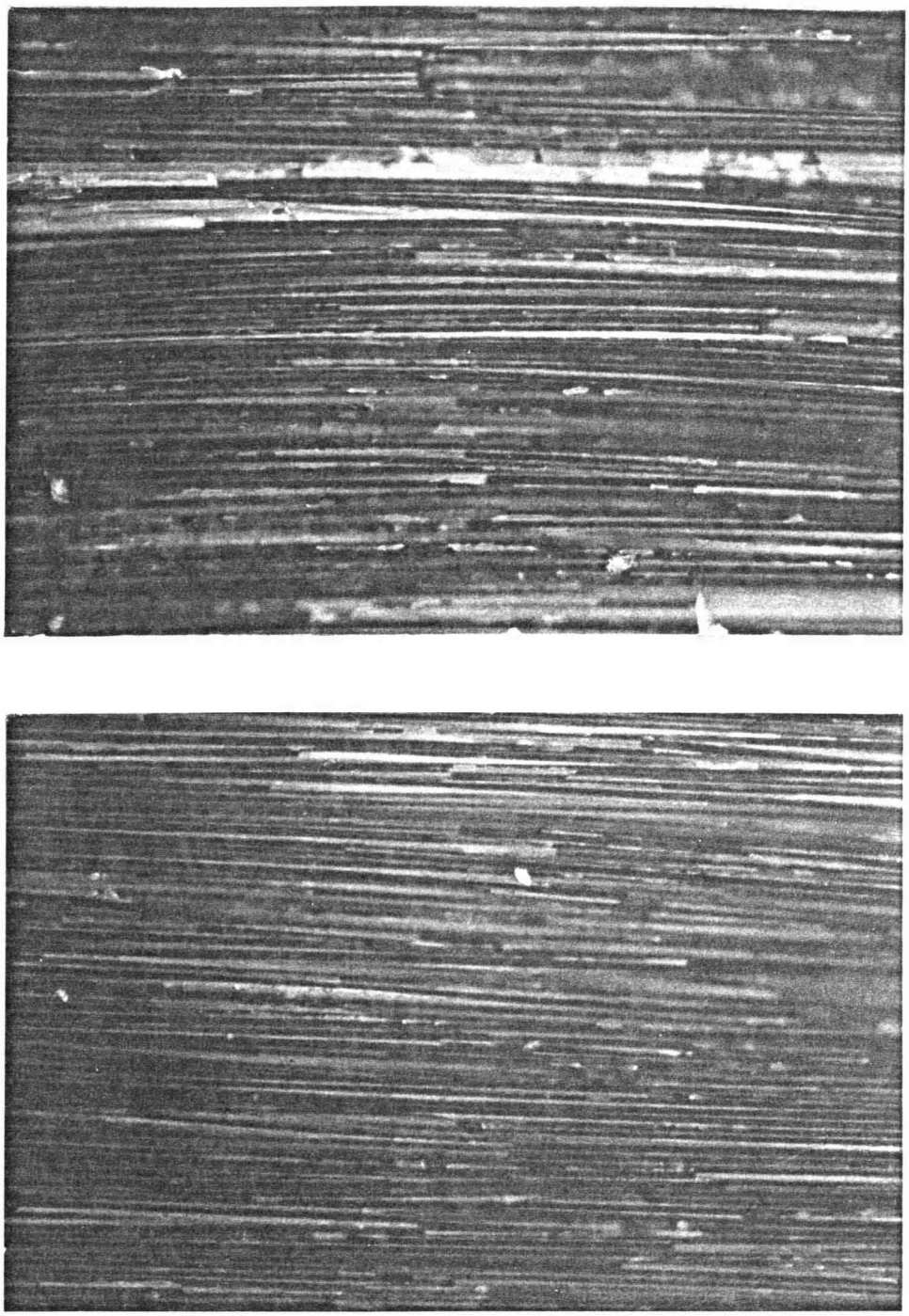

Figure 36. 100X; Fluores; BP907 - TYPE A - 1. Typical adhesive fracture surface where failure has occurred at the interface between the long fibers and the matrix resin leaving bare long fibers.

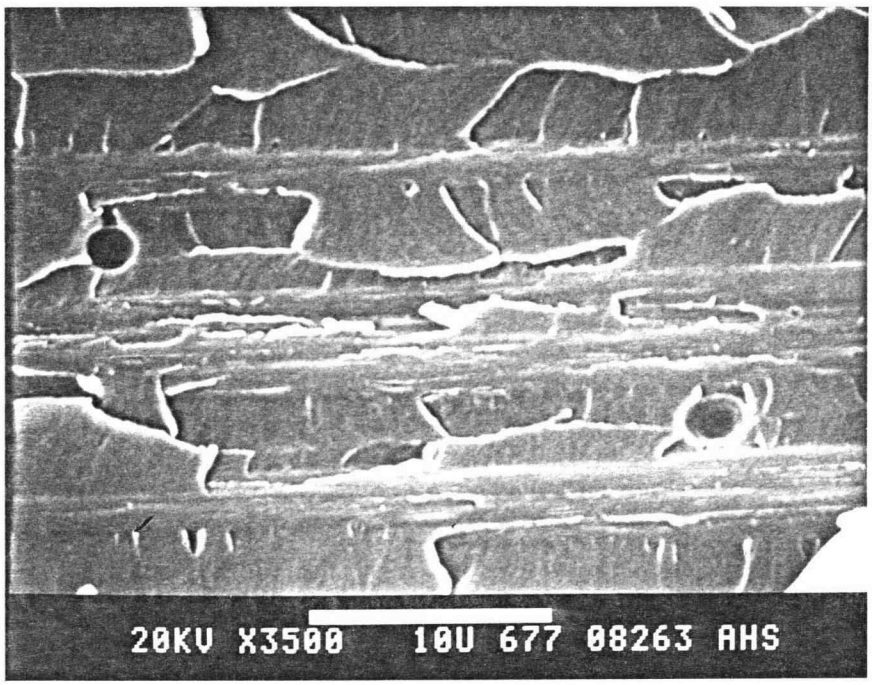

Figure 37. 3500X; SEM; BP907 - TYPE M - 2. Mode I fracture surface showing a hole (left) and a dimple (right) where the elastomeric modifiers were resident in the resin matrix. This additive was dispersed in the resin in the BP907 system only. Crack movement was from left to right as can be seen by the resin pile-up on the left side of the hole.

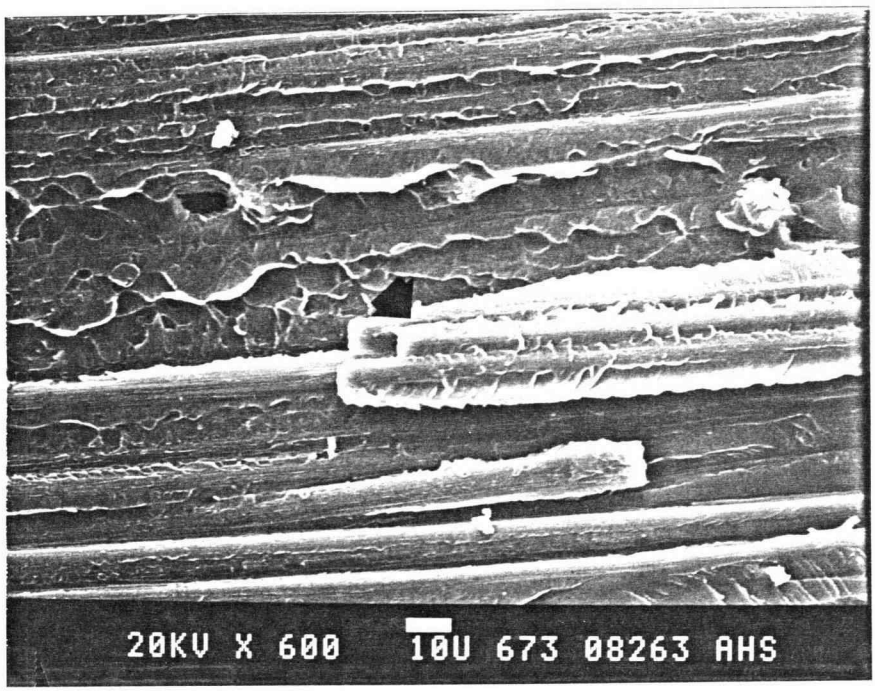

Figure 38. 600X; SEM; BP907 - TYPE H - 3. Microphotograph showing the remnant from a tie zone as a result of mode I crack propagation within the interlaminar layer. The pointer indicates a fiber bundle which was attached to the opposite face of the DCB specimens fractured surface. Note how well the resin has adhered to the long graphite fibers. Also visible in this photograph is a hole where a fiber was pulled from (upper left). Crack movement was from left to right.

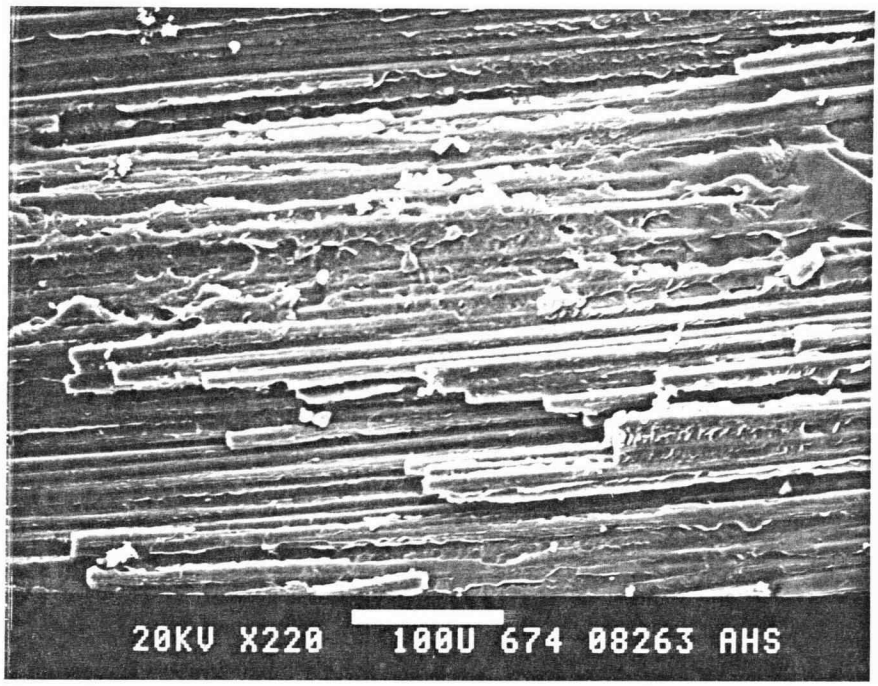

Figure 39. 220X; SEM; BP907 - TYPE H - 3. SEM photograph showing the lifted and broken fibers as a result of a tie zone in the vicinity of a crack arrest point (mode I). Note how well the resin adheres to the fibers. Also note the aggressive nature of the resin fracture which was audible during testing. Crack movement was from left to right.

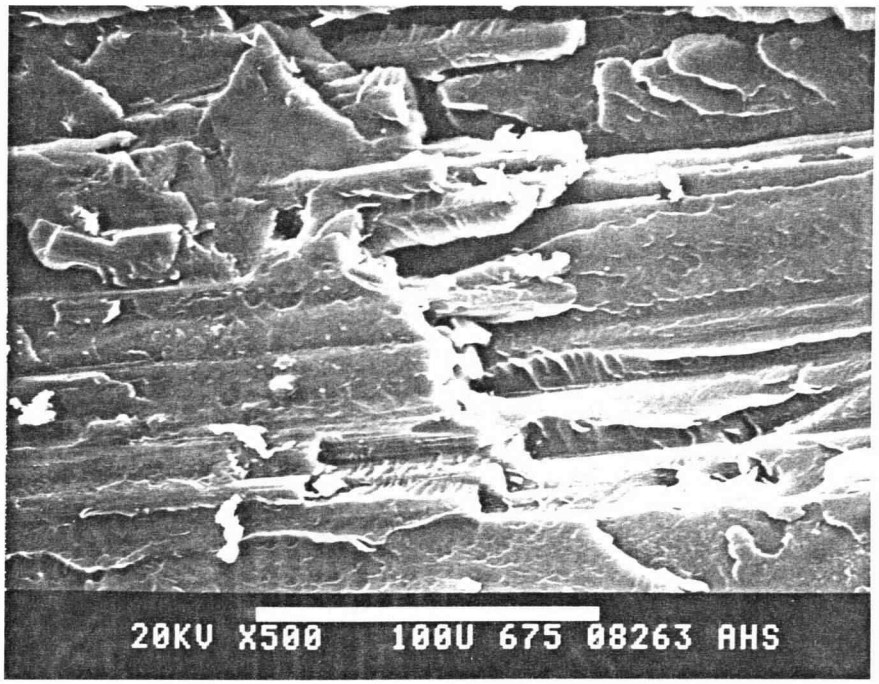

Figure 40. 500X; SEM; BP907 - TYPE H - 3. This picture shows the edge of a resin plateau produced by the arrest of a long crack jump. The resin plateau appears as a crack beach mark when viewed from a lower magnification and spans the entire width of the specimen surface. Crack movement was from left to right.

Crack Propagation Interactions

Crack propagation through the interlaminar layer of the composite systems studied resulted in a number of different phenomena. As mentioned above, several observations regarding surface appearance can be made owing to the mode I type of crack growth. Other conclusions can be drawn in relation to how the moving crack front interacts with the microstructure to dissipate its energy.

One of the manifestations of crack growth is the ever changing nature of its movement. During testing, a noticeable difference exists between stable or sudden crack growth and audible or silent crack growth. Presumably, the nature of movement is due to crack-microstructure interactions. Stable crack growth probably happens when the crack is propagating easily in its plane without severe obstruction. Sudden crack growth would likely occur when the crack front is attempting to change its plane of growth. Considering the ovservation that crack propagation generally tries to avoid fiber interactions[23], stable or sudden growth is a possible function of the concentration of fibers ahead of the crack front.

Another manifestation of crack propagation through the interlaminar layer of the composites studied is that of a fiber tie-zone. A tie-zone occurs when long fibers link across the crack from one beam half to the other as shown is Figure 41. Tie-zones presumably result when crack propagation leaves the original interlaminar layer and runs in a plane of predominantly continuous fibers. Continued crack propagation past the tie-zone inevitably breaks the continuous fibers in that zone after which the remnants of

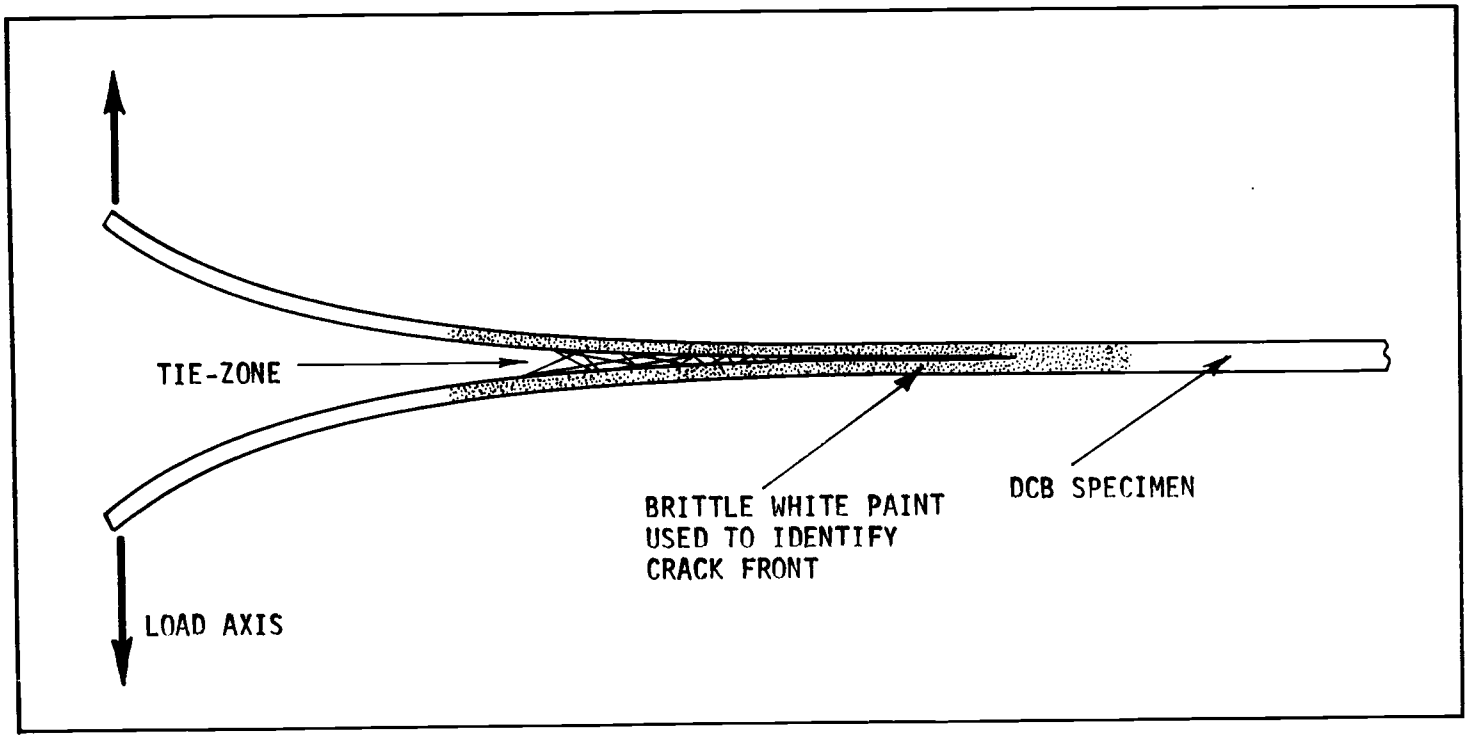

Figure 41. Sketch of tie-zone development across a crack front. The tie zone results from the crack possibly leaving the interlaminar layer (or the layer being too thin) and intercepting long fibers which then tie across the crack.

the tie-zone can be observed on the failed surface (Figure 38 and 39).

Crack Front Identification

During testing, the growth of the crack in the interlaminar layer is monitored visually on the side of the specimen. As the crack propagates and separates the two beam halves, its progression is noted by the separation of a brittle white paint on the side of the specimen. Post fracture examination found that this method was exceptionally accurate for determining the location of the crack-front at the edge of the specimen. The assumption was made that the crack-front has no curvature; that is, marking the crack at its edge is as good as marking it at its center. The true crack-front in most cases is slightly curved in the direction of its movement. The difference in measuring the crack-front at its edge or at its tip is never more than 2 millimeters. The actual distance of crack jump in either case is the same.

Surface examinations of the specimens tested in this study found that the crack-front arrest point could be determined in many instances. Examinations under the microscope revealed that the crack-front arrest point was sometimes noticeable due to the presence of a beach mark that extended the width of the specimen. Seldom was this beach mark straight or continuous. Figures 42 and 43 show these beach marks. This type of surface feature is very difficult to photograph even though they are clearly visible by eye. Beach marks are the actual crack-fronts at arrest.

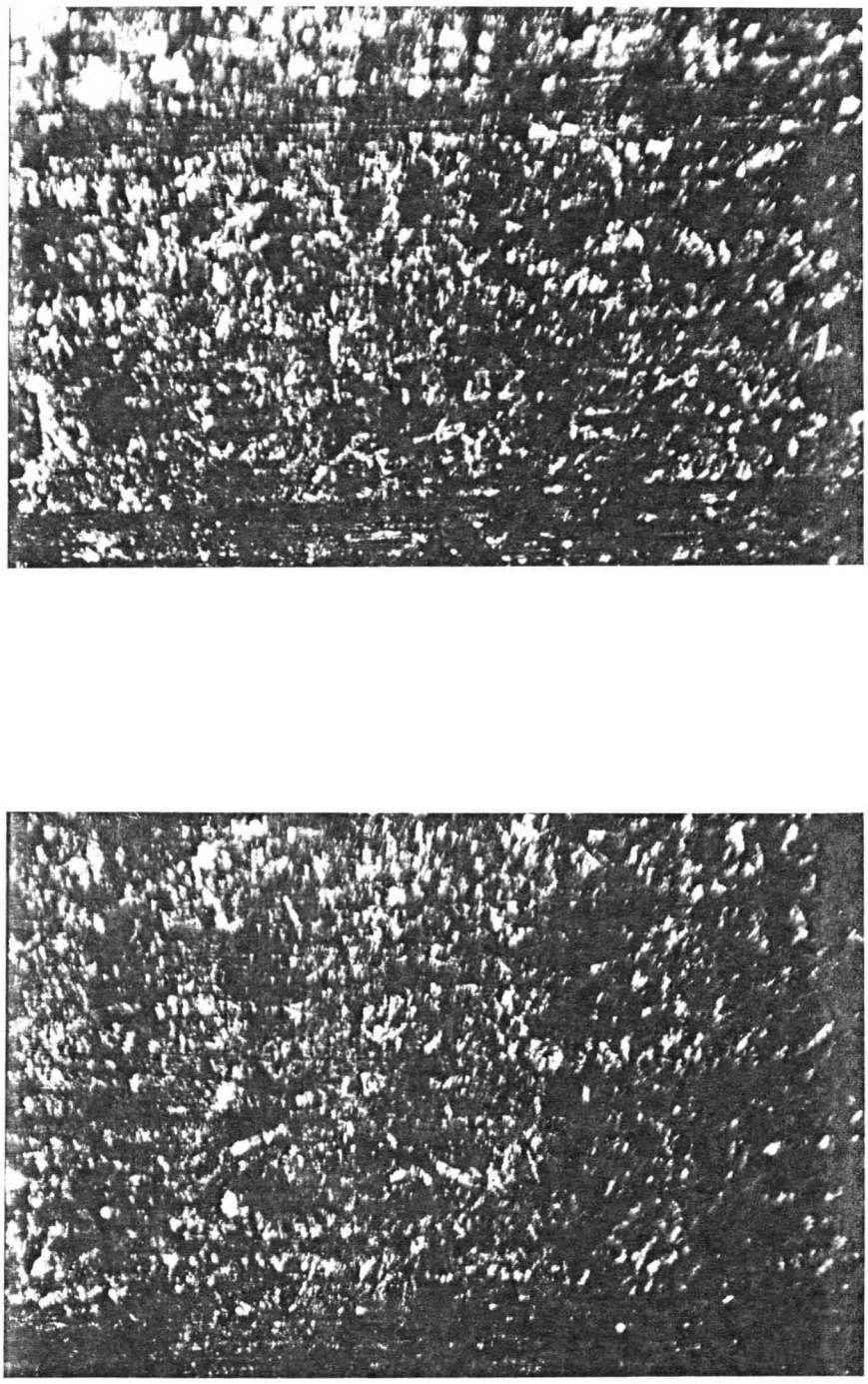

Figure 42. 63X; Incident Light; BP907 - TYPE H - 3. Two photographs showing beach marks as a result of the crack-front arrest.

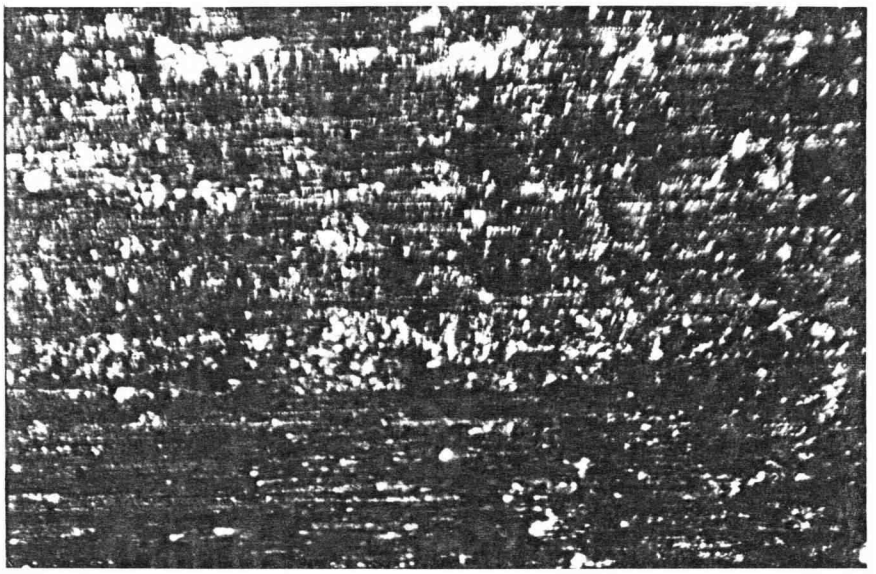

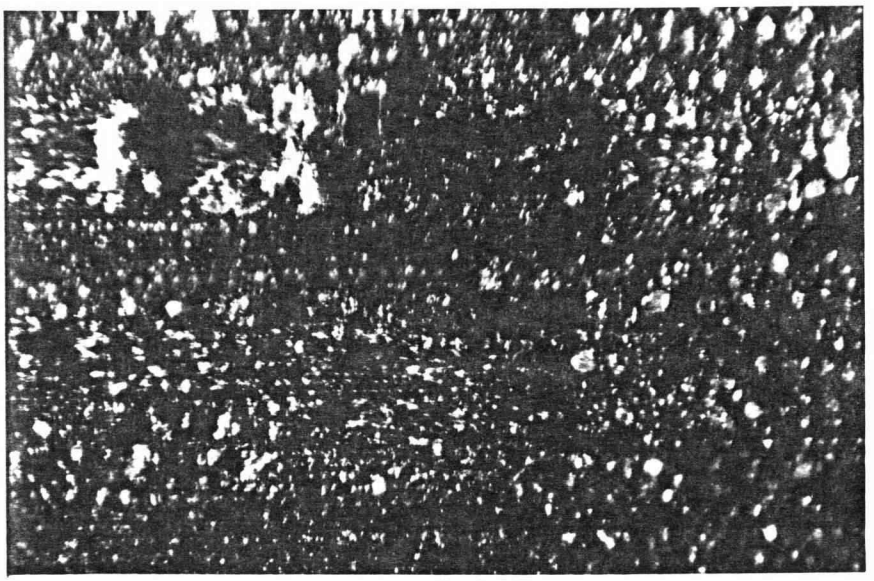

Figure 43. 63X; Incident Light; 984 - TYPE F - 1. Two photographs showing beach marks as a result the crack-front arrest.

Interlaminar Layer Appearance

Most research leading to the analysis and understanding of fracture in laminated composites is predicated on the assumption of a interlaminar layer of constant thickness and uniform dimension, when in fact this is not always the case. Several spot checks of the layer thickness of the composites used in this study revealed variations from 1 to 50 micrometers. Variations in the thickness also leads to variation in the planeness of the layer, and consequently, variation in the planeness of the propagating crack. Figure 44 shows a typical specimen and how the resin and fibers are arranged. Uniformity of the interlaminar layer thickness is important when considering possible delaminations, voids, or points of weaknesses which may result from an interlaminar layer being resin rich or resin starved.

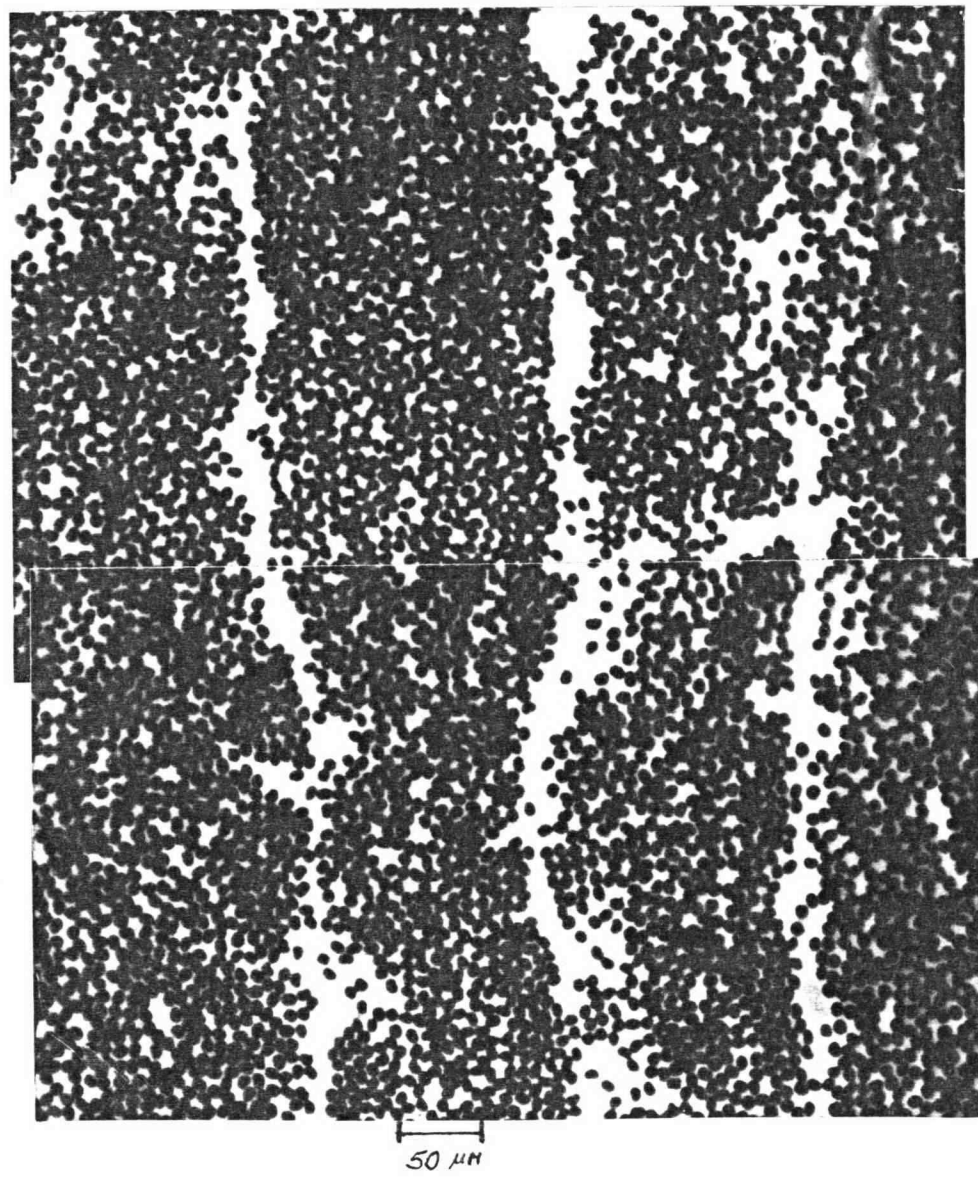

Figure 44. 160X; Fluores; BP907 - TYPE A - 2. Photograph taken from the polished end of the specimen looking in the direction of the long fiber axis. This view is representative of most specimens showing the individual plies, their distribution, and the variation of the interlaminar layer.

Conclusions

Considering the evidence presented in the preceeding sections the following conclusions may be drawn. First, the J integral is revealed to be a more applicable fracture parameter considering the nonlinear behavior of the composite materials examined, and the unwarranted assumptions in the linear isotropic G analysis. The fact that the composite specimens tested in this study do not behave according to small deflection, linear beam bending theory (e.g. increasing E) substantiates this conclusion. The compliance calibrated approach turns out to be a good estimate which is close in value to that given by the J integral method. However, for materials that exibit higher degrees of nonlinearity than observed in this study, the compliance calibrated G approach may result in a considerable overestimate or underestimate of critical failure energy.

Second, the occurence of a permanent deformation brings up several questions regarding the nature of DCB testing and fracture toughness testing in general. This permanent deformation was observed after a number of repetitive tests were performed on the same specimen. During testing, the matrix and fibers at the interlaminar surface near the crack tip are subjected to extremely high stresses due to the moment arm of the DCB specimen. These high stresses may result in matrix cracking or fiber and matrix slippage thus causing the permanent deformation. If not accounted for the permanent deformation will add to the area under the load-displacement curves thus giving a misrepresentation of critical failure energy.

A third conclusion is that for materials that exibit high degrees

of plasticity the DCB specimen as used in this study may or may not yield an accurate representation of critical failure energy. For these types of materials the shape of the load-deflection curve has been known to change depending on the materials past loading history. With this in mind, any specimen which requires a fatigue type loading to initiate a crack would be suspect when determining critical failure energies of highly plastic materials. Past loading history is an important concept which should always be recognized before evaluating material properties.

Finally, microscopic examination revealed that mode I crack propagation results in a relatively smooth planar fracture surface as crack growth tends to remain in the interlaminar layer. The observed beach marks on each specimen indicate that the method used to measure crack growth (e.g. visually on the edge of the painted specimen) was exceptionally accurate for determining the location of the crack front.

Bibliography

1. American Society for Testing and Materials. 1980. Standard test for plane-strain fracture toughness of metallic materials. Book of ASTM Standards, Part 10, E 399-78a, 580-601.

2. Barten, H.J. 1944. On the deflection of a cantilever beam. Quarterly of Applied Mathematics, Vol. II, No. 2: 168-171.

3. Barten, H.J. 1945. On the defelction of a cantilever beam. Quarterly of Applied Mathematics, Vol. III, No. 2: 275-276.

4. Begley, J.A. and J.D. Landes. 1972. The J intergral as a fracture criterion. Fracture toughness, Proceedings of the 1971 National Symposium of Fracture Mechanics, Part II, ASTM STP 514, 1-20.

5. Bisshopp, K.E. and D.C. Drucker. 1945. Large deflection of cantilever beams. Quarterly of Applied Mathematics, Vol. III, No. 3: 272-275.

6. Brock,D. 1982. Elementary engineering fracture mechanics. 3rd edition, Martinus Nijhoff Publishers.

7. Brown, W.F. Jr. and J.E. Srawley. 1966. Plane strain crack toughness testing of high strength metallic materials, ASTM STP 410, Philadelphia.

8. Chow, C.L. and K.M. Ngan. 1978. Effect of large rotation of DCB specimen on fracture toughness evaluation. International Journal of Fracture, Vol. 14: R277-R279.

9. Chow, C.L. and C.W. Woo. 1980. Fracture studies with DCB specimen. International Journal of Fracture, Vol. 14: 39-58.

10. Cohen, R.N. 1982. Effect of resin toughness on fracture behavior of graphite/epoxy composites. Masters thesis, Texas A & M University.

11. Devitt, D.F., R.A. Schapery and W.L. Bradley. 1980. A method for determining the mode I delamination fracture toughness of elastic and viscoelastic composite materials. Journal of Compostie Materials, Vol. 14: 270-285.

12. Griffith, A.A. 1921. The phenomena of rupture and flow in solids. Phil. Trans. Royal Soc. London, Ser. A, Vol. 221: 163-198.

13. Griffith, A.A. 1924. In "Proceedings of the First International Congress of Applied Mathematics, "Delft. pp.55.

14. Hoagland, R.G. 1967. On the use of the double cantilever beam specimen for determining the plane strain fracture toughness of metals. Journal of Basic Engineering: 525-532.

15. Ilcewicz, L.B. 1984. The relationship between wave dispersion and fracture strength. PhD Thesis, Oregon State University.

16. Inglis, C.E. 1913. Proceedings, Institute of naval architects, Vol. 55: p. 219.

17. Irwin, G.R. 1957. Analysis of stresses and strains near the end of a crack traversing a plate. Journal of Applied Mechanics. Vol. 9: p. 361.

18. Jurf, R.A. and R.B. Pipes. 1982. Interlaminar fracture of composite materials. Journal of Composite Materials, Vol. 16: 386-394.

19. Landes, J.D. and J.A. Begley. 1972. The effect of specimen geometry on J_{Ic}. Fracture toughness, Proceedings of the 1971 National Symposium on Fracture Mechanics, Part II, ASTM STP 514, pp. 24-39.

20. Landes, J.D. and J.A. Begley. 1977. Recent developments in J_{Ic} testing, in developments in fracture mechanics test methods standardization, ASTM STP 632, pp. 57-81.

21. Lewis, B. and F. Monasa. 1981. Large deflections of cantilever beams of nonlinear materials. Computers and Structure, Vol. 14, No. 5-6: 357-360.

22. Lo, C.C. and S. Das Gupta. 1978. Bending of a nonlinear rectangular beam in large defelction. Journal of Applied Mechanics, Vol. 45: 213-215.

23. Mandell, J.F., D.D. Huang and F.J. McGarry. 1982. Crack propagation modes in injection molded fiber reinforced thermoplastics, in short fiber reinforced composite materials, ASTM STP 772, pp. 3-32.

24. Matthews, J.R. and G.D. West. 1983. J_{Ic} measurement point determination for HY 130, CMS-9, and Inconel alloy 718. Journal of Testing and Evaluation, Vol. 11, No. 3: 217-224.

25. Monasa,F. and G. Lewis. 1983. Large defelctions of point loaded cantilvers with nonlinear behavior. Journal of Applied Mathematics and Physics, Vol. 34: 124-130.

26. Mostovoy, S., P.B. Crosley, and E.J. Ripling. 1967. Use of crack-line-loaded specimens for measuring plane-strain fracture toughness. Journal of Materials, Vol. 2, No. 3: 661-681.

27. Orowan, E. 1955. Energy criteria of fracture. Welding Journal, Vol. 34: 157-160.

28. Paris, P.C. 1977. Fracture mechanics in the elastic-plastic regime, in flaw growth and fracture, ASTM STP 631,pp. 3-27.

29. Prathap, F. and T.K. Varadan. 1976. Journal of Applied Mechanics, Transactions of the ASME, December, pp. 689-690.

30. Rice, J.R. 1968. A path independent intergral and the approximate analysis of strain concentrations by notches and cracks. Journal of Applied Mechanics, Transactions of the ASME, June, pp. 379-386.

31. Rice, J.R. 1968. Mathematical analysis in the mechanics of fracture, in Fracture, H. Liebowitz, ed., Vol. 2, Academic press, New York, pp. 191-311.

32. Rybicki, E.F., D.W. Schmueser, and J. Fox. 1977. An energy release rate approach for stable crack growth in the free-edge delamination problem. Journal of Composite Materials, Vol. 2: 470-487.

33. Sidey,G.R. and F.J. Bradshaw. 1971. Some investigation on carbon-fibre-reinforced plastics under impact loading, and measurements of fracture energies, in carbon fibers: their composites and applications, Proceeding of the international conference organized by the Plactic's Institute of London on February 2,3,4, 1971. Copyright by the Plastic's Institute.

34. Sik,G.C. and H. Liebowitz. 1968. Mathematical theories of brittle fracture, in Fracture, H. Liebowitz, ed., Vol. 2, Academic press, New York, pp. 68-188.

35. Srawley,J.E. and W.F. Brown. 1965. Fracture toughness testing methods, ASTM STP 632, pp. 57-81.

36. Tada,H., P.C. Paris, and G.R. Irwin. 1973. The stress analysis of cracks handbook. Del Research Corp., Hellertown, PA.

37. Wang, S.S., J.F. Mandell, and F.J. McGary. 1978. An analysis of the crack tip stress field in DCB adhesive fracture specimans. International Journal of Fracture, Vol. 14: 39-58.

38. Wang, S.S. 1980. An analysis of delamination in angle-ply fiber-reinforced composites. Journal of Applied Mechanics, Vol. 47: 64-70.

39. Wang, S.S. 1983. Fracture mechanics for delamination problems in composite materials. Journal of Composite Materials. Vol. 17: 210-223.

40. Westergaard, H.M. 1939. Bearing pressures and cracks. Transactions of the ASME, Vol. 61, pp. A-49 - A-53.

41. Wigotsky, V. 1981. Advanced fibers are catching on. Design Engineering, October : 45-51.

42. Wilkins, D.J., J.R. Eisenmann, R.A. Camin, W.S. Margolis, and R.A. Benson. 1982. Characterizing delamination growth in graphite-epoxy, in damage in composite materials, ASTM STP 775, pp. 168-183.

43. Wu, E.M. 1968. Fracture mechanics of anisotropic plates, in composite materials workshop. S.W. Tsai, J.C. Halpin, and N.J. Pagamo, ed., Technomic Publishing Co., Conn, pp. 20-43.

44. Vanderkley, P.S. 1981. Mode I - Mode II delamination fracture toughness of a unidirectional graphite/epoxy composite. Texas A & M University report MM 3724-81-15.

45. Zweben, C., W.S. Smith, M.W. Wardle. 1979. Test methods for fiber tensile strength, composite flexural modulus, and properties of fabric-reinforced laminates, in composite materials: testing and design, ASTM STP 674, pp. 228-262.